

Streaming potential coupling coefficient of quartz glass bead packs: Dependence on grain diameter, pore size, and pore throat radius

Paul W. J. Glover¹ and Nicholas Déry¹

ABSTRACT

The Helmholtz-Smoluchowski (HS) equation is commonly used to relate the streaming potential coupling coefficient of rocks to their zeta potential, pore fluid dielectric permittivity, conductivity, and viscosity despite it being known for almost 80 years that it does not work well for porous media. One of the problems is that the HS equation contains no implicit dependence on grain size, pore size, or pore throat size. Another has been the lack of high-quality data relating the streaming potential coupling coefficient to rock microstructural parameters. In this, predominantly experimental work, we have measured the streaming potential coupling coefficient for 12 sizes of quartz glass beads and two fluid salinities. A comparison of the new data and the existing data with the conventional HS equation and Revil's grain size-dependent HS model shows the grain size-

dependent model to be far superior in describing the data. Recognizing their utility in reservoir characterization, we have developed new equations that describe how the streaming potential coupling coefficient varies with pore diameter and pore throat diameter. We have compared experimental determinations as a function of pore throat diameter with these new relationships and found them to work very well if the ratio of the mean pore diameter to the pore throat diameter is 1.662, which is valid for random arrangement of monodisperse spheres. The zeta potential has also been calculated from the grain size-dependent HS equations and are found to be approximately constant and in agreement with the theoretically predicted values. The equations presented in this paper allow the streaming potential coupling coefficient of a reservoir rock to be calculated as a function of grain size, pore size, and pore throat size.

INTRODUCTION

This paper presents new streaming potential coupling coefficient data as a function of grain size to a literature that is almost devoid in such data. It is important to do this for two reasons. First, electrokinetic measurements are beginning to be used in many aspects of reservoir engineering, such as downhole seismoelectric imaging (e.g., Dupuis et al., 2009; Glover and Jackson, 2010) and the prediction of water encroachment near producing oil wells (e.g., Jaafar et al., 2009; Glover and Jackson, 2010). These applications need reliable ways of calculating the streaming potential coupling coefficient of rocks. Second, one of the most common ways of describing a reservoir rock is by its grain size (although pore size and pore throat size are perhaps even more useful). Hence, if we can find a way of relating the streaming potential coupling coefficient of a rock to its mean grain size, pore size, or pore throat size, we will have useful tools for predicting the streaming potentials in our reservoirs. However, as we show clearly later in this paper, the grain size effect is only important

for reservoirs that are saturated with low-salinity fluids.

In this paper, we examine the new and existing data in the light of the classical HS equation and its grain size-dependent modification in both its exact form (Revil et al., 1999b) and an approximate form that stems from Glover et al. (2006), as well as deriving and testing new equations for the streaming potential coupling coefficient as a function of pore size and pore throat size.

The streaming potential coupling coefficient of capillary tubes is known to be governed by the classical Helmholtz-Smoluchowski (HS) equation (e.g., Overbeek, 1952; Hunter, 1981; Maineult et al., 2004; Bolève et al., 2007; Saunders et al., 2008), which is given in its simplest form in equation 1 by

$$C_s = \frac{\Delta V}{\Delta P} = \frac{\varepsilon_r \varepsilon_0 \zeta}{\eta \sigma_f^*}, \quad (1)$$

where the streaming potential coupling coefficient C_s (in V/Pa) is the ratio of the measured streaming potential ΔV (in V) to the applied

Manuscript received by the Editor 25 September 2009; revised manuscript received 8 June 2010; published online 20 December 2010.
¹Département de géologie et de génie géologique, Université Laval, Québec, Canada. E-mail: paglover@ggl.ulaval.ca; nicholas.dery.1@ulaval.ca.
© 2010 Society of Exploration Geophysicists. All rights reserved.

fluid pressure difference ΔP (in Pa) that drives the fluid through the capillary tube. This value depends on the dielectric permittivity of the fluid $\epsilon_f = \epsilon_r \epsilon_o$ (in F/m), the fluid viscosity η (in Pa.s), the fluid conductivity σ_f^* (in S/m) and the zeta potential ζ (in V). The zeta potential is the electric potential on the shear plane when a part of the diffuse layer is transported by fluid flow (Glover and Jackson, 2010). Early tests of the HS equation as a function of capillary diameter were carried out by White et al. (1932a; 1932b; 1936).

The classical HS equation is commonly applied to porous media including rocks even though it has never been validated for these media since there exists no independent measurement of the zeta potential for complex porous media. Indeed, the equation is generally used to calculate the zeta potential of porous media from measured values of streaming potential. However, significant errors can arise from the use of the wrong values in the parameters equation 1, which are discussed in the following few paragraphs.

First, most researchers take a value of $\epsilon_f = \epsilon_r \epsilon_o = 80 \times 8.854 \times 10^{-12}$ F/m (e.g., Revil et al., 1999a; 1999b), corresponding to an aqueous bulk fluid at about 25 °C. However, the value of ϵ_r in the fluid diminishes within the diffuse layer as one approaches the mineral surface, taking values as low as 5 near the Stern Plane (Grahame, 1950). Pride and Morgan (1991) indicate that the effect is negligible for most bulk electrolyte solutions, but more research needs to be carried out as the diminution of the dielectric permittivity occurs near the solid-liquid interface, which is where the electrokinetic coupling occurs.

Second, if the HS equation is not being used to calculate the zeta potential, but the zeta potential is one of its input parameters, one must also be careful about the pH. Like the dielectric permittivity, the fluid pH varies as one approaches the mineral surface (Revil and Glover, 1997). For silica surfaces, the pH becomes more acidic. It is known that the zeta potential depends strongly on pH (Somasundaran and Kulkarni, 1973; Morgan et al., 1989; Lorne et al., 1999; Guichet and Zuddas, 2003), its magnitude decreasing as one approaches the point of zero charge of the system (Ishido and Mizutani, 1981). For silica in aqueous solutions $\text{pH}_{\text{pzc}} \approx 3$. Since the shear plane is very near the surface (the distance of the shear plane from the Stern plane is $\chi_\zeta = 3 \times 10^{-10}$ m (Revil and Glover, 1997)), the use of a zeta potential for $\text{pH} = 7$ would probably be inappropriate, with a smaller value of pH being preferable. We have no current mechanism for making this adjustment because the pH dependency in the surface conduction theory of Revil and Glover (1997) and Revil et al. (1999b) only accounts for pH variation in the bulk fluid.

The third problem is more tractable. The valid fluid conductivity σ_f^* in the HS equation is not that of the bulk fluid. This is because it is not just the bulk fluid that is moved during the fluid flow that creates the streaming potential; the mobile parts of the diffuse layer are also transported (e.g., Pride and Morgan, 1991). Hence, in equation 2, we can express the fluid conductivity as partly due to the bulk fluid with an additional surface conductance term

$$\sigma_f^* = \sigma_f + \sigma_s = \sigma_f + 2 \frac{\sum_s}{\Lambda}, \quad (2)$$

where σ_s is the surface conductivity (in S/m), \sum_s is the specific surface conductance (in S) and Λ is a characteristic length scale that describes the size of the pore network (in m) (e.g., Ishido and Mizutani, 1981; Morgan et al., 1989). This is a linear (Waxman and Smits type) summation of the bulk and surface conductivities. If this correction is omitted for streaming potentials in capillary tubes, the error is not

usually important because the bulk conductivity dominates the conductivity term except for very small capillaries filled with very low-salinity solutions (White et al., 1932a; 1932b; 1936). However, in rocks it is extremely important to take the correction into account, especially when the pore size distribution presents very small values.

The pore size (and by extension the grain size) also controls the permeability of a porous medium. Hence, one would expect there to be a link between the streaming potential coupling coefficient and permeability that is mediated by surface conductance and the rock microstructure. A link between streaming potential coupling coefficient and permeability has been noted by a number of authors (Jouniaux and Pozzi, 1995a; 1995b; Lorne et al., 1999), which is interesting because such a link, if fully understood theoretically, might allow us to estimate the permeability of reservoirs remotely. Already relationships that have their origin in the electrical and electrokinetic theory of porous media have been used to find permeability as a function of grain size (Glover et al., 2006) and pore size as a function of grain size (Glover and Walker, 2009).

To summarize, traditionally, the HS equation is seen as being composed of three parameters that depend on the fluid alone (*viz.*, the fluid dielectric permittivity, the fluid viscosity, and the fluid conductivity) and one that depends on the rock (*i.e.*, the zeta potential). The control of the streaming potential coupling coefficient exercised by the rock structure was imagined to reside solely in the zeta potential value. Now, it is possible to take a different view. Both the fluid dielectric permittivity and the fluid conductivity have a contribution from the bulk fluid and another due to the presence of the diffuse layer at its interface with the rock structure, while the zeta potential is modified by a fluid pH that changes due to its proximity to that same interface.

It should be pointed out rather strongly that the calculated values of zeta potential for porous media in the literature may be significantly in error because of errors in the input parameters. Consequently, we recommend that the zeta potential calculated from the HS equation should always be quoted together with the values of ϵ_r , η , σ_f^* and pH that were used to calculate it.

Although the surface dielectric permittivity effect, surface pH effect, and surface conductivity effect are often regarded as secondary and negligible, this paper shows that at least the surface conductivity effect in porous rocks can be extremely significant when the fluid conductivity is low, and makes the streaming potential coupling coefficient a function of the grain size of the rock.

We start by reviewing the exact and approximate solutions of the relationship between streaming potential coupling coefficient and grain size that arose from the work of Revil et al. (1999a), Revil (2002), and Glover et al. (2006) in the light of two of the existing data sets (Bull and Gortner, 1932; Bolève et al., 2007). Subsequently, we derive new relationships for the streaming potential coupling coefficient as a function of pore size. We then describe our experimental methodology. We discuss our new experimental data: first as a function of grain size, comparing it with the model of Revil et al. (1999a) and Revil (2002); second as a function of pore size using the models newly developed earlier in this paper; and last as a function of pore throat size using models also newly developed in this paper. We then invert our new streaming potential coupling coefficient versus grain size data to obtain the zeta potential as a function of grain size and flow rate, and compare the zeta potential so-calculated with those available from existing theoretical models.

GRAIN SIZE DEPENDENCE

Equation 1 shows no dependence of streaming potential coupling coefficient on either pore or grain size. However, when one combines it with equation 2, a characteristic length scale associated with the rock microstructure Λ is introduced in the fluid surface conduction term. There have been several models that relate the characteristic length scale Λ to grain diameter and to pore diameter in the last 10 years. One was provided by [Revil et al. \(1999a\)](#)

$$\Lambda = \frac{d}{3(F-1)}, \quad (3)$$

where d is the mean grain diameter (in m) and F is the formation resistivity factor of the rock. If we take equations 1–3 together, in equation 4 we get

$$C_s = \frac{\Delta V}{\Delta P} = \frac{d\epsilon_f\zeta}{\eta_f(d\sigma_f + 6\Sigma_s(F-1))}. \quad (4)$$

The streaming potential coupling coefficient is directly proportional to the dielectric permittivity and to the zeta potential. Although the dielectric permittivity varies with frequency, temperature, and pressure, it can usually be taken to be constant for any given reservoir rock at a certain depth. The zeta potential can vary over at least one order of magnitude, and is dependent on both on pore fluid concentration and pH, as well as a set of electrochemical constants that are constant for a given mineral and a given temperature. Hence, the zeta potential can also usually be taken to be constant for any given reservoir rock at a given depth (i.e., constant for a given set of thermodynamic conditions, matrix, and pore fluid). The streaming potential coupling coefficient is inversely proportional to the pore fluid viscosity, and although viscosity varies with salinity and temperature, it, too, can be taken to be constant for a given reservoir rock at a given depth. The dependence on grain size (and pore and pore throat size as we shall see later) is more complex. It is only developed for fluids of low salinity, and the degree of its development depends on the relative values of the surface conductivity and the bulk fluid conductivity. It becomes negligible as $\sigma_f \gg 6\Sigma_s(F-1)$, which is about $\sigma_f \gg 18\Sigma_s$ for monodisperse spherical beads. The formation factor for spherical beads is about 4 because the appropriate cementation exponent is 1.5 ([Sen et al., 1981](#); [Glover and Walker, 2009](#)) and the porosity of the random pack of monodisperse spherical beads is about 0.4. This will be discussed in detail in the experimental results. Here the bulk conductivity and surface conductivity also depend on temperature, salinity, and pH, and the surface conductivity depends additionally on a set of electrochemical constants that are constant for a given mineral and temperature.

More recently, [Revil and Cathles \(1999\)](#) and [Glover et al. \(2006\)](#) independently produced a different expression given by

$$\Lambda \approx \frac{d}{2mF}, \quad (5)$$

where m is the cementation exponent of the rock (no units).

If we take equations 1, 2, and 5 together, we get

$$C_s = \frac{\Delta V}{\Delta P} = \frac{d\epsilon_f\zeta}{\eta_f(d\sigma_f + 4\Sigma_s mF)}. \quad (6)$$

Reference to Equation A-10 of [Glover et al. \(2006\)](#) shows equation 5 to be an approximation of $\Lambda = d/2m(F-1)$, which is valid in the limit $F \gg 1$, and which corresponds to equation 23 of [Revil \(2002\)](#). For the case of monodisperse spherical particles, where $m = 1.5$ ([Sen et al., 1981](#); [Glover and Walker, 2009](#)), equation 5 and equation 3 are the same providing $F \gg 1$. For this reason, for the rest of this paper we will call equation 4 the exact solution and we will call equation 6 the approximate solution. It should be pointed out that there is no advantage to using the approximate solution for packs of monodisperse spherical particles because for $m = 1.5$, the formation factor F is approximately 4, which is not sufficiently larger than unity for the approximation to be valid. However, for real rocks with formation factors in the range 10 to 100, the approximate solution is valid.

It can quickly be seen that equations 4 and 6 are very similar and are sensitive in the same way to changes in their input parameters. In the case of equation 6, the grain size dependence becomes negligible for $\sigma_f \gg 4\Sigma_s mF$, which is approximately $\sigma_f \gg 24\Sigma_s$ for monodisperse spherical beads.

The main advantage of equations 4 and 6 is that we can use them to examine the variation of streaming potential coupling coefficient with grain size. A more substantial step forward theoretically would be to develop equations as a function of pore size and pore throat size as they would have direct application in the hydrocarbon industry. This has been carried out in a section toward the end of this paper.

Figure 1 shows the only substantial streaming potential coupling coefficient versus grain size data available in the scientific literature ([Bull and Gortner, 1932](#); [Bolève et al., 2007](#)), together with the results of equations 4 and 6. Figure 1a shows the data from [Bull and Gortner \(1932\)](#) with the results of equations 4 and 6. A similar diagram using only equation 4 is present in [Revil et al. \(1999a\)](#). It is clear that these sparse data fit either of the models well at a surface conductance of about 4×10^{-9} S, and the blind application of the classical HS relationship (equation 1) leads to a constant value of 25.04 V/MPa irrespective of the grain size. The coefficients of determination for the fit of equations 4 and 6 to the [Bull and Gortner \(1932\)](#) data using the quoted experimental conditions and a surface conductance of $\sigma_s = 4 \times 10^{-9}$ S were $R^2 = 0.926$ and $R^2 = 0.890$, respectively. Hence, the classical model is not a good fit to the data. Indeed, for a grain size of 5 μm , [Bull and Gortner \(1932\)](#) measured streaming potential coupling coefficient of about 5 V/MPa, which represents an overestimation by the classical HS equation of 400%, and for smaller grain sizes than 5 μm , the misfit would be even greater.

Figure 1b shows the streaming potential coupling coefficient calculated with equation 4 and equation 6 as a function of grain size and with variable surface conductance. It is clear that when the surface conductance is small ($\Sigma_s = 10^{-11}$ S), the errors associated with not taking into account the surface conductance are small for a grain sizes of about 1 μm and at larger grain sizes they become negligible. As the surface conductance increases, the effect becomes more pronounced with significant reductions in the streaming potential coupling coefficient below that predicted by the classical HS model occurring at larger and larger grain sizes. For example, with $\Sigma_s = 10^{-8}$ S, the streaming potential coupling coefficient for a grain size of 100 μm is about 12 V/MPa — half that predicted by the classical HS equation. Values in this range are common for both clean and clayey rocks ([Revil and Glover, 1998](#); [Leroy and Revil, 2004](#)). Hence, it is extremely important that a streaming potential

model that takes account of the grain size variation is used in any modeling.

Figure 1c shows the streaming potential coupling coefficient measurements for seven grain sizes and six pore fluid conductivities made by Bolève et al. (2007). These potentially important data unfortunately contain quite a lot of scatter. The error bars in the abscissa are the range of grain diameters quoted by Bolève et al. (2007). There were no ordinate errors quoted in the paper. We have applied a $\pm 20\%$ error in an attempt to quantify the degree of scatter in the data. The models shown in Figure 1c are those calculated using equation 4 with $m = 3.4$, $\phi = 0.4$, $F = 3.37$, $\text{pH} = 5.75$, $T = 25^\circ\text{C}$, which are the mean values calculated from Bolève et al. (2007), the zeta potential is calculated from the empirical fit given by Bolève et al. (2007) in their Figure 8. The surface conductance is $\Sigma_s = 3.95 \times 10^{-9}$ S, which is that given by Bolève et al. (2007) in their Figure 4, and is close to that derived by Revil et al. (1999b). These curves approximately match the magnitude and the trend of the experimental data, being constant and equal to the classical HS result at large grain sizes, and decreasing as grain size diminishes; that for $\sigma_f = 3$

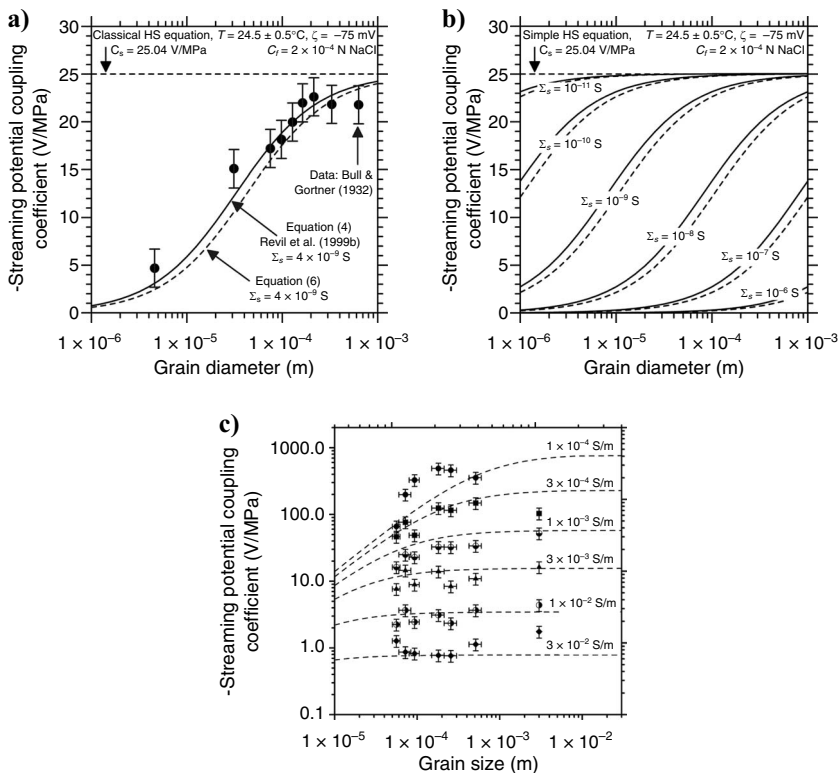


Figure 1. (a) Streaming potential coupling coefficient as a function of grain diameter. The symbols represent experimental data (Bull and Gortner, 1932). The solid line shows the model of Revil et al. (1999a) in its exact form (equation 4), and the dashed line represents its approximate form after Glover et al. (2006) (equation 6). (b) Streaming potential coupling coefficient as a function of grain size for a range of different values of surface conductance, with curves defined as in Figure 1a. (c) Streaming potential coupling coefficient as a function of grain diameter for the experimental data of Bolève et al. (2007) for seven bead diameters and six pore fluid conductivities (σ_f). Symbols: solid lozenges, $\sigma_f = 3 \times 10^{-2}$ S/m; vertically partitioned circles, $\sigma_f = 1 \times 10^{-2}$ S/m; solid triangles, $\sigma_f = 3 \times 10^{-3}$ S/m; horizontally partitioned circles, $\sigma_f = 1 \times 10^{-3}$ S/m; solid squares, $\sigma_f = 3 \times 10^{-4}$ S/m; solid circles, $\sigma_f = 1 \times 10^{-4}$ S/m. The curves are the result of equation 4 with $m = 3.4$, $\phi = 0.4$, $F = 3.37$, $\zeta = 0.0146 + 0.0291 \times \log_{10}(\sigma_f)$, $\Sigma_s = 4 \times 10^{-9}$ S, $T = 25^\circ\text{C}$ and $\text{pH} = 5.75$. The large grain diameter asymptote represents the result of applying the classical HS model.

$\times 10^{-4}$ S/m being the best of the six fluids. However, the data are not of sufficiently high quality to form a valid test for equation 4, and no formal statistical tests of goodness of fit have been carried out.

There are a few other sources of streaming potential coupling coefficient data as a function of grain size. Ahmad (1964) carried out tests on 3 mm and 6 mm diameter glass beads as well as three sieved fractions of St. Peter sand (125 to 177 μm , 350 to 420 μm , 590 to 840 μm) for two salinities. He found that the streaming potential coupling coefficient increased as grain size decreased, which is contrary to the findings of other researchers. A review of his experimental techniques has not indicated an explanation for the discrepancy. A few years later Ogilvy et al. (1969) used what seems to be the same type of apparatus to measure six sieved fractions of "practically clean" Moskva river sand with mean diameters between 100 μm and 2000 μm saturated with an aqueous solution of 10^{-3} N NaCl. This time the streaming potential coupling coefficient increased nonlinearly from about 4 V/MPa until about 8 V/MPa as the grain size decreased from 2000 μm to about 300 μm , then sharply decreased again, reaching about 5.5 V/MPa for the smallest grain size fraction (100 to 160 μm).

Another early publication on glass beads also contains conflicting data (Schriever and Bleil, 1957). Although these three studies are not consistent wholly with each other, they are also very different from the data of Bull and Gortner (1932) and Bolève et al. (2007).

Since the Bull and Gortner (1932) and Bolève et al. (2007) data sets are too sparse and imprecise to test equations 4 and 6, we have carried out a suite of experimental measurements on quartz glass beads with a wide range of diameters and for only two fluid salinities, but with a focus on producing the highest quality data possible. These data are discussed later in this paper.

PORE SIZE DEPENDENCE

Most recently, it has also been possible to take account of the mean pore radius r (in m) of the porous media using the expression

$$\Lambda = r \sqrt{\frac{a}{8}}, \quad (7)$$

which arises from the mean grain diameter to mean pore size conversion method by Glover and Walker (2009). Equation 7 collapses to $\Lambda = r$ if a is set equal to 8, which corresponds to Λ being equal to the radius of a capillary tube (e.g., Li et al., 1995). For a wide range of porous media, including reservoir rocks, the value of a is thought to be constant and equal to about 8/3. This parameter is formally the same as the m -value used by Pride (1994) in his equations for the AC streaming potential coupling coefficient (note that this value is not the same as the cementation exponent of a rock and to avoid ambiguity we have called it m^* in this work).

$$L(\omega) = L_o \left[1 - i \frac{m^* \omega}{4 \omega_t} \left(1 - 2 \frac{\tilde{d}}{\Lambda} \right)^2 \times \left(1 - i^{3/2} \tilde{d} \sqrt{\frac{\omega \rho_f}{\eta_f}} \right) \right]^{-1/2}, \quad (8)$$

Here in equation 8, Pride uses $L(\omega)$ to represent the frequency dependent phenomenological coefficient and $L_o = \epsilon_r \epsilon_o \zeta / \eta$ is its zero frequency limit, ω is the frequency (in rad/s or Hz) and ω_t the transition frequency (in the same units as ω), m^* is Pride's m constant (no units), ρ_f is the density of the fluid (in kg/m³), and \tilde{d} is the characteristic length associated with the width of the double layer (in m). Since $\tilde{d} \ll \Lambda$ for most geological regimes, the correction term is small under the thin double layer assumption.

Taking equations 1, 2, and 7 together leads to

$$C_s = \frac{\Delta V}{\Delta P} = \frac{r \epsilon_f \zeta \sqrt{a}}{\eta_f (r \sigma_f \sqrt{a} + 4 \Sigma_s \sqrt{2})}, \quad (9)$$

and if $a = 8/3$

$$C_s = \frac{\Delta V}{\Delta P} = \frac{r \epsilon_f \zeta}{\eta_f (r \sigma_f + 2 \Sigma_s \sqrt{3})}. \quad (10)$$

Equations 9 and 10 can be used to describe how the streaming potential coupling coefficient varies with the mean pore radius r .

EXPERIMENTAL METHODOLOGY

A range of silica glass beads from several different manufacturers was used (Table 1). In all cases, the beads were thoroughly washed several times in distilled water and acetone before being left to air

dry in a dust-free environment. Most of each sample was then left to equilibrate in the aqueous fluid in which it was to be measured. A randomly sampled portion of each sample of beads was analyzed using optical microscopy, image analysis, and a Malvern laser diffraction particle size analyzer to know accurately the mean diameter of each set of beads and the variability in the diameter. Table 1 shows the main characteristics of the bead packs. Figure 2 shows the bead diameter distributions, where the symbols are the measurements and the lines are the best fitted log-normal curves according to the standard equation

$$P(d) = \frac{1}{\sigma_o d \sqrt{2\pi}} \exp\left(-\left[\frac{\ln(d/d_o)}{\sigma_o \sqrt{2}}\right]^2\right), \quad (11)$$

where $P(d)$ is the probability of obtaining a certain grain diameter d (m), d_o (in m) is the mean grain diameter, and σ_o (no units) is the standard deviation of the variable's natural logarithm.

The beads were packed into the Perspex cell shown in Figure 3 while under the saturation fluid in order to ensure that there were no air bubbles in the sample. The sample cell tube was made of Perspex with an internal diameter of 1 cm, and was long enough to accommodate samples up to 5 cm long. Each end was supplied with a National Pipe Thread Tapered Thread thread to which two manifolds were screwed using a Polytetrafluoroethylene tape seal. The manifolds were constructed from nylon Swagelok® fittings. These fittings are not available commercially. We constructed our fittings by cutting off one arm of a nylon Swagelok crosspiece (NY-200-4), and cutting the Swagelok connector off a nylon Swagelok NPT straight adaptor (NY-200-1-2). We then polished the cut faces and carefully glued the now three-armed Swagelok crosspiece to the NPT thread to form the required manifold, without blocking the flow paths. The straight adaptor was also drilled out to provide a larger diameter for fluid flow. The beads were held in place in the tube by fine nylon

Table 1. Overview of sample properties.

Sample number	Grain diameter (laser) ($\times 10^{-6}$ m)	Mean pore diameter (corrected) ($\times 10^{-6}$ m)	Mean pore throat diameter (Hg) ($\times 10^{-6}$ m)	Porosity (He) (-)	Porosity (Hg) (-)	Formation factor ($m = 1.5$) (-)	Permeability (measured) ($\times 10^{-12}$ m ²)
1	1.05	0.32	0.17	0.411	0.377	3.80	0.00057
2	2.11	0.61	0.33	0.398	0.380	3.98	0.00345
3	5.01	1.35	0.99	0.380	0.362	4.27	0.0181
4	11.2	3.28	1.62	0.401	0.383	3.94	0.0361
5	21.5	5.88	3.91	0.383	0.370	4.23	0.228
6	31.0	8.80	5.36	0.392	0.380	4.07	0.895
7	47.5	14.03	7.96	0.403	0.395	3.91	1.258
8	104	29.73	19.90	0.394	0.382	4.04	6.028
9	181	52.08	35.30	0.396	0.390	4.01	21.53
10	252	77.60	44.00	0.414	0.410	3.75	40.19
11	494	133.29	82.60	0.379	0.375	4.28	224.0
12	990	273.23	163.00	0.385	0.379	4.18	866.7
Mean				0.395	0.382	4.04	

The grain diameter is the modal value from laser diffraction measurements. The mean pore diameter is calculated using the techniques in Glover and Walker (2009). Parameters marked "He" were made using helium porosimetry, and those marked "Hg," by mercury porosimetry. The formation factor was calculated from the helium porosity assuming $m = 1.5$.

meshes, which were sometimes supplemented by filter paper for the smaller bead sizes. A blank test showed that the meshes and filter paper did not contribute to the streaming potential signal.

Fluid was flowed through the sample for several hours in either direction to ensure that the beads were well equilibrated with the saturating fluid and that all concentration gradients that could give rise to an electrochemical potential were removed. The experience of [Leroy et al. \(2008\)](#) was that the pH of the fluid increased from pH = 7 to pH = 9.24 and the fluid conductivity increased to 1.03×10^{-2} S/m when deionized water was added to glass beads. This was not our experience, where the pH remained essentially unaltered at pH = 6.9 for the 2×10^{-4} mol/L NaCl and pH = 6.8 for the 2×10^{-3} mol/L NaCl, and the fluid conductivities remaining stable at 2.44×10^{-3} S/m and 2.410×10^{-2} S/m, respectively, and which are in good agreement with the fluid conductivity for NaCl at 25 °C obtained from the model of [Sen and Goode \(1992\)](#). We attribute the pH and conductivity stability of our measurements to the successive washings that the beads had undergone and suggest that fine glass dust associated with the beads was the source of the efficient apparent bead dissolution observed by [Leroy et al. \(2008\)](#).

The temperature of the cell was also measured to ensure that any thermoelectric contribution to the measured potential was minimized. However, because the sample is small and the thermal mass of the fluid reservoir is correspondingly large, we found that by keeping the fluids at 25 °C before the measurement ensured that the entire experiment held that same value very accurately throughout the streaming potential measurements.

Fluid was flowed through the sample in both directions at up to four rates between 0.1 and 499 ml/hr using a Pharmacia P500 twin bore piston pump for the larger flow rates and a gravity feed for the smaller flow rates, and choosing the flow rates to produce measurable pressure drops across the sample. Figure 4 shows a typical measurement as a function of flow rate. Indeed, one of the challenges of these experiments is the large range of fluid permeabilities, pressure drops, and streaming potentials measured. Most of the pressure measurements were made using standard 300 psi (2 MPa) gauge pressure transducers obtainable from Omega (PX302-300GV). For the lowest pressure differences, the difference between the levels in two columns of water was also used as this method, though seemingly crude, can provide very accurate differential pressure measurements for pressure differences less than 10 kPa. The streaming potentials were measured using two matched miniature Ag-AgCl nonpolarizing electrodes from Cypress Systems, which were placed just outside the flow and opposite the pressure measurement at each end of the sample. The potential measurement was carried out with a Keithley 2000 microvoltmeter with an accuracy of $\pm 0.002\%$. The zero offset of the pressure transducers and the voltmeter were measured

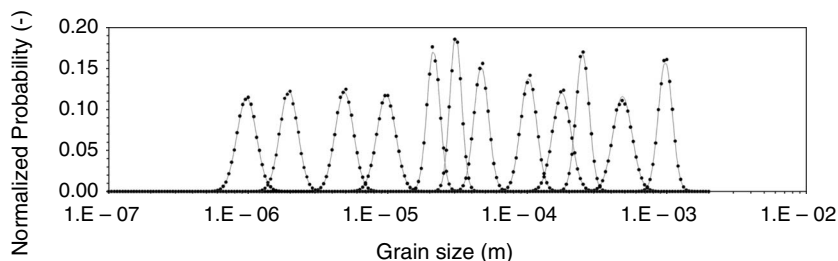


Figure 2. The grain size distributions used in the experimental measurements. The symbols represent the measured values and the lines represent the best fit log-normal curves.

at the beginning and end of each measurement. The offset was removed from the data by subtracting the value at the beginning of each measurement. The drift was removed from the data by subtracting values that were calculated by interpolating linearly between the measurements at the beginning and end of each set of measurements as a function of time. However, drift was always very low — less than 0.5% of the measured values. A small earthed Faraday cage was used to surround the sample during measurement. Additionally, the electrical conductivity of each sample was measured while there was no flow, and the fluid permeability was measured at each of the flow rates.

In these measurements, the fluid flow was imposed and the permeability was calculated from the measured flow rate and the consequent pressure drop. This is, of course, experimentally equivalent to imposing a pressure gradient and then calculating the permeability from the measured pressure drop and consequent fluid flow. It should be mentioned that in nature flow is normally driven by pressure gradients. This is perhaps a fine distinction and should not make any difference to the results of the research providing that the flow remains within the laminar regime. There is increasing evidence that the streaming potential coupling coefficient is perturbed by turbulent and transitional flow for which the Reynolds number $Re > 1$ ([Watanabe and Katagishi, 2006](#); [Kuвано et al., 2006](#); [Bolève et al., 2007](#)). In this paper, the Reynolds number varies from $Re_{\min} = 3.71 \times 10^{-10}$ for the smallest spheres at the lowest flow rate to $Re_{\max} = 3.49 \times 10^{-3}$ for the highest grain size at the highest flow rate, both of which fall well within the laminar range.

At the end of the experiment, the samples were weighed, flushed with methanol, dried, and weighed again. The masses were used in conjunction with the previously measured fluid density and cell parts to calculate the porosity of the sample. The entire sample, still enclosed in its Perspex tube and connectors was sent to an external service company to be submitted to mercury porosimetry using a Micromeritics porosimeter, which provides the porosity of the sample as well as its pore throat size spectrum.

EXPERIMENTAL RESULTS

Grain size dependence

Figure 5 shows the streaming potential coupling coefficients of a range of quartz glass bead packs as a function of the mean diameter of the glass bead. The horizontal error bars represent the equivalent standard deviation of the log-normally distributed grain size diameter measurements. We have chosen not to show error bars for the vertical direction. Instead, all the data points are shown as open symbols. This shows the total range of the measurements. At least eight measurements (different flow rates and flow direction) were carried out for each bead pack. The errors associated with the measurements are much smaller than those of [Bull and Gortner \(1932\)](#) or those implied by the scatter in the data of [Bolève et al. \(2007\)](#) because we spent considerable efforts improving the signal-to-noise ratio of very small voltage measurements made with small pressure differences, and by using high-quality and very expensive quartz glass beads. Mean values of the measured streaming potential coupling coefficients are also shown numerically in Table 2.

The experimental measurements have been

compared with the results of the exact solution of the theoretical equations by [Revil et al. \(1999a\)](#) and [Revil \(2002\)](#) (equation 4) and the approximate form that is given by equation 6. Although this sounds straightforward, it is quite complex because our intention is to provide a theoretical fit where there are no adjustable parameters. In the following theoretical approach, high-quality theoretical val-

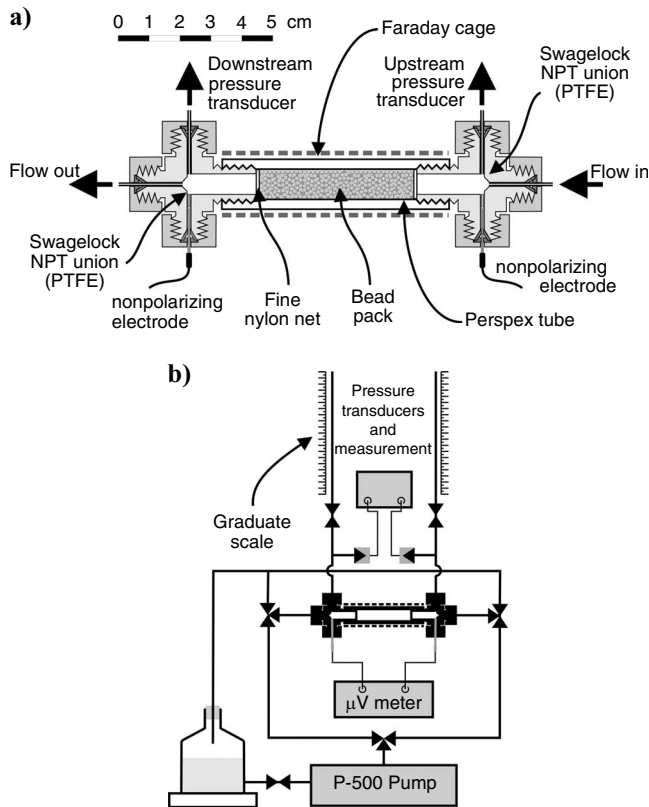


Figure 3. (a) The experimental cells used in this work. Note that the input and output manifolds are constructed from two separate connectors that are commercially available in nylon from Swagelok Inc. Once the experiment is finished, these end-pieces can be unscrewed and replaced by a simple inexpensive plug for transport or storage. (b) The flow diagram showing how the fluids were passed through the sample cells.

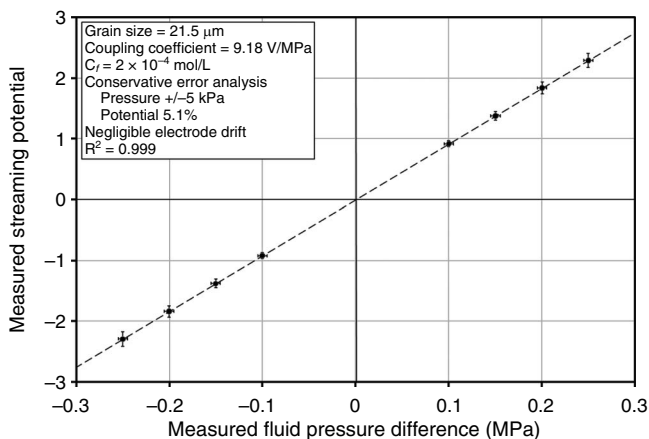


Figure 4. A typical measurement of streaming potential made as a function of flow rate with four flows in each direction. Please note that the flow rate was adjusted until chosen pressure differences were attained, whereon the streaming potential was measured.

ues for all the parameters in equations 4 and 6 have been found, and compared with experimentally determined values whenever possible.

It might be said that for a model that contains many parameters, a fit is almost always possible. However, the methods set out in this paper are not simply fitting equations — they are theoretical relationships that are based on the physics of the system in which we do not have the luxury of being able to drop, add, or modify parameters on an ad hoc basis. The theoretical parameters are constrained to fall within certain ranges that are more or less well defined experimentally. By taking each parameter individually, we will show that the streaming potential coupling coefficients calculated in this paper are based on the following extremely well-constrained physical parameters.

Temperature. — The temperature of the experiment was controlled by the process fluid that had been stabilized for at least

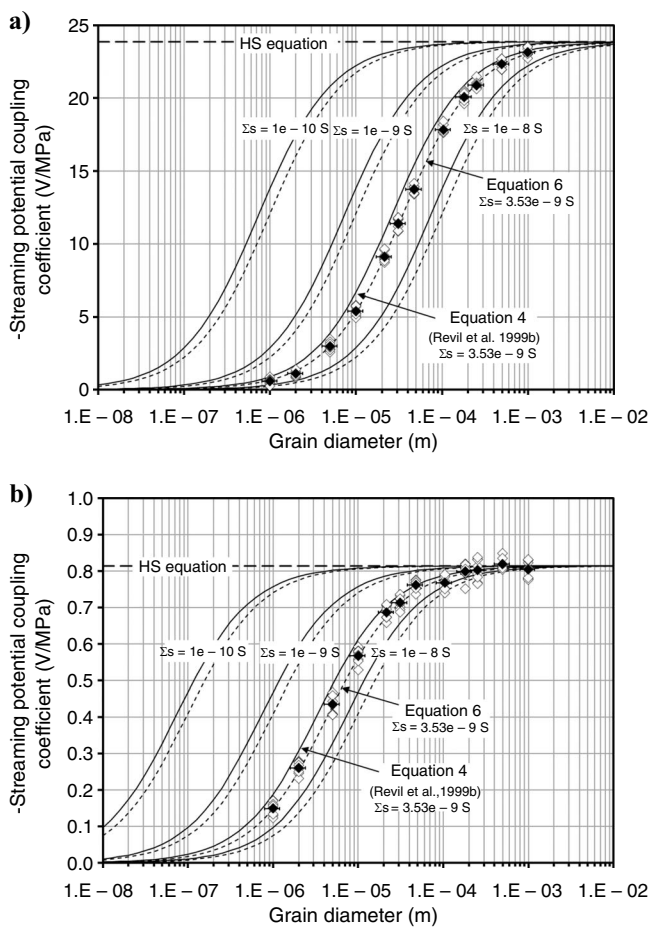


Figure 5. Streaming potential coupling coefficients of a range of quartz glass bead packs as a function of the mean diameter of the glass beads. (a) Pore fluid salinity $C_f = 2 \times 10^{-4}$ mol/L, (b) Pore fluid salinity $C_f = 2 \times 10^{-3}$ mol/L. The open symbols show the streaming potential coupling coefficient measurements for individual flow rates at a given grain size, which indicates their uncertainty. The solid symbol shows the mean value calculated from the gradient of plots like that shown in Figure 4. The horizontal error bar shows the effective standard deviation of the laser diffraction bead size measurements. The solid line shows the model of [Revil et al. \(1999a\)](#) in its exact form (equation 4), and the dashed line represents its approximate form after [Glover et al. \(2006\)](#) (equation 6).

48 hours at a set temperature in the same temperature-controlled chamber that was used for the experiments. The temperature was determined experimentally using glass immersion thermometers before and after the experiment, and the stability of the temperature was measured with type K and PT100 temperature transducers during the experiments. For all experiments $T = 25 \pm 0.5^\circ\text{C} = 298.15 \pm 0.5\text{ K}$.

Pore fluid salinity. — The pore fluids were made extremely carefully using deionized water and Analar grade solute, and ensuring that all latent heat of dissolution had dissipated before measuring the fluid volume. Two pore fluids were used, one with $C_f = 2 \times 10^{-4}\text{ mol L}^{-1}$, and the other with $C_f = 2 \times 10^{-3}\text{ mol L}^{-1}$. The first was chosen to coincide with that of Bull and Gortner (1932) so that the results could be compared.

Grain size. — Experimentally determined values from the laser diffraction particle size analyzer were used. The peak grain size values are shown in Table 1.

Electrical permittivity. — The relative permittivity ϵ_r (no units) was determined using Olhoeft's equation (Olhoeft, unpublished note, 1980; Revil et al., 1999a) in equation 12

$$\epsilon_r(T, C_f) = a_0 + a_1T + a_2T^2 + a_3T^3 + c_1C_f + c_2C_f^2 + c_3C_f^3, \quad (12)$$

where $a_0 = 295.68$, $a_1 = -1.2283\text{ K}^{-1}$, $a_2 = 2.094 \times 10^{-3}\text{ K}^{-2}$, $a_3 = -1.41 \times 10^{-6}\text{ K}^{-3}$, $c_1 = -13.00\text{ L mol}^{-1}$, $c_2 = 1.065\text{ (L mol}^{-1})^2$, $c_3 = -0.03006\text{ (L mol}^{-1})^3$, T is in kelvin and the equation is valid in the range from 273 K to 373 K and C_f is the salinity of the bulk pore fluid in mol L^{-1} . The permittivity in vacuo $\epsilon_0 = 8.854 \times 10^{-12}\text{ F/m}$. The decrease in permittivity near the surface occurs on the scale of a few angstroms (Grahame, 1947; Booth, 1951; Hunter, 1966; Pride and Morgan, 1991). Since the Debye screening length for the two pore fluid concentrations used in this paper are at least 10 times as thick, we have assumed them to be negligible. Mixing calculations using the method of Iglesias and Péon Fernández (2001) support this assumption.

Dynamic viscosity. — The dynamic viscosity η_f of the pore fluid (in Pa.s) was calculated using the Phillips et al. (1978) equation

$$\eta_f(T, C_f) = e_1 + e_2 \exp(\alpha_1 T) + e_3 \exp(\alpha_2 C_f^m) + e_4 \exp(\alpha_3 T + \alpha_4 C_f^m), \quad (13)$$

where $e_1 = 4.95166 \times 10^{-5}\text{ Pa.s}$, $e_2 = 6.034658 \times 10^{-4}\text{ Pa.s}$, $e_3 = 9.703832 \times 10^{-5}\text{ Pa.s}$, $e_4 = 1.025107 \times 10^{-3}\text{ Pa.s}$, $\alpha_1 = -0.06653081^\circ\text{C}^{-1}$, $\alpha_2 = 0.1447269\text{ molal}^{-1}$, $\alpha_3 = -0.02062455^\circ\text{C}^{-1}$, $\alpha_4 = 0.1301095\text{ molal}^{-1}$, T is in $^\circ\text{C}$ and C_f^m is the molality of the bulk pore fluid. Since our solutions are weak, it is possible to say that $C_f^m = C_f$ and consequently to use salinity in mol L^{-1} in place of molality in equation 13. Viscoelectric effects have been assumed to be negligible in accordance with the results of Lyklema and Overbeck (1961), Hunter (1966), and the interpretation of Pride and Morgan (1991).

Cementation exponent. — This parameter is constant for spheres at $m = 1.5$ (Sen et al., 1981; Glover and Walker, 2009). The cementation exponent is related to the degree of connection enjoyed by the

pores. Parallel tubes have a cementation exponent of unity whereas most sandstones fall in the range 1.6 to 2.0. Carbonate rocks often have large pores that are not well connected and, hence, have higher cementation exponents.

Porosity. — The theoretical value for a random packing of spherical beads of the same size is $\phi_r = 0.399$ (Wyllie and Gregory, 1955; Guéguen and Palciauskas, 1994). We have used this value, and found that it is in good agreement with the porosity measurements that we made on the bead samples (mean values $\phi_{\text{Helium}} = 0.395$, $\phi_{\text{Hg}} = 0.382$).

Formation factor. — This is given by Archie's law (Archie, 1942) as $F = \phi^{-m}$. For spheres it takes the value $F = 3.9677$.

Electrical conductivity of the bulk fluid. — We have used the Sen and Goode (1992) equation to provide the electrical conductivity of the bulk solution (in S/m) in equation 14

$$\sigma_f(T, C_f) = (d_1 + d_2T + d_3T^2)C_f - \left(\frac{d_4 + d_5T}{1 + d_6C_f} \right) C_f^{3/2}, \quad (14)$$

where $d_1 = 5.6$, $d_2 = 0.27$, $d_3 = -1.51 \times 10^{-4}$, $d_4 = 2.36$, $d_5 = 0.099$, $d_6 = 0.214$, T is in $^\circ\text{C}$ and C_f is the salinity of the bulk pore fluid (mol L^{-1}). We also measured the conductivity of the pore fluids with a bench top conductivity meter and a Solartron 1260A Frequency Response Analyzer and found them to be in extremely good agreement with the theoretical values. For solutions of $C_f = 2 \times 10^{-4}$ and $C_f = 2 \times 10^{-3}\text{ mol L}^{-1}$, the experimental values were $\sigma_f = 2.44 \times 10^{-3}$ and $\sigma_f = 2.43 \times 10^{-2}\text{ S/m}$, respectively, and the theoretical values were $\sigma_f = 2.4376 \times 10^{-3}$ and $\sigma_f = 2.410 \times 10^{-2}\text{ S/m}$, respectively.

Zeta potential. — This parameter was calculated in equations 15–17 using the techniques described in Revil and Glover (1997) and in Revil et al. (1999b). The zeta potential is given by

$$\zeta = \varphi_d \exp(-\chi_\zeta / \chi_d) \quad (15)$$

where

$$\chi_d = \sqrt{\frac{\epsilon_0 \epsilon_r k_b T}{2000 N e^2 I}} \quad (16)$$

and

$$\varphi_d = \frac{2k_b T}{3e} \ln \left(\frac{\sqrt{8 \times 10^3 \epsilon_r \epsilon_0 k_b T N} (10^{-pH} + K_{Me} C_f)}{2e \Gamma_s^o K_{(-)}} \times \left[\frac{C_f + 10^{-pH}}{\sqrt{\frac{1}{2} \sum_i^n Z_i^2 C_i^f}} \right] \right) \quad (17)$$

Here we have used the following parameters that are consistent with

the symbols used in [Revil et al. \(1999b\)](#):

$\chi_\zeta = 3 \times 10^{-10}$	Distance of the shear plane from the bead surface	(m)	Revil and Glover (1997)
χ_d	Debye screening length	(m)	Equation 16
$k_b = 1.38 \times 10^{-23}$	Boltzmann's constant	(J/K)	Lide (2009)
$e = 1.602 \times 10^{-19}$	Elementary charge	(C)	Lide (2009)
$N = 6.022 \times 10^{23}$	Avagadro's constant	(mol ⁻¹)	Lide (2009)
$K_{Me} = 10^{-3.25}$	Binding constant for cation (sodium) adsorption on quartz	(-)	Revil et al. (1999b)
$K_{(-)} = 10^{-7.5}$	Disassociation constant for dehydrogenization of silanol surface sites	(-)	Hiemstra et al. (1989a; 1989b)
$pH = 6.9$	Measured with a bench top meter	(-)	Experimentally measured
C_a	Acid concentration	(mol L ⁻¹)	$C_a = 10^{-pH}$
$Z_i = 1$	Valence of the ionic species <i>i</i>	(-)	Lide (2009)
$C_i^f = C_f$	Concentration of ionic species <i>i</i>	(mol L ⁻¹)	Set experimentally
I	Ionic strength	(mol L ⁻¹)	Set experimentally
$\Gamma_s^\circ = 2.6 \times 10^{18}$	Surface site density	(m ²)	Joergensen and Tovborg-Jensen (1967)

Although the fundamental constants are known to great accuracy, there is some considerable uncertainty over the exact value of other parameters such as χ_ζ , K_{Me} , $K_{(-)}$, and Γ_s° . The values that we have used here are based on the full discussion that is available in [Revil et al. \(1999b\)](#).

The value of the Debye screening length arrived at in this work were 2.147×10^{-8} m and 6.79×10^{-9} m for fluid concentrations of 2×10^{-4} mol L⁻¹ and 2×10^{-3} mol L⁻¹, respectively, which are both much larger than the position of the shear plane from the surface that was taken as 3×10^{-10} m after [Revil and Glover \(1997\)](#). Because the thickness of the diffuse layer may be considered to be twice

the Debye length, we can see that the great majority of the double layer is moved during electrokinetic coupling (that between 3×10^{-10} m and 4.294×10^{-8} m from the surface for a bulk fluid concentration of 2×10^{-4} mol L⁻¹, and that between 3×10^{-10} m and 1.36×10^{-8} m from the surface for a bulk fluid concentration of 2×10^{-3} mol L⁻¹).

The Bjerrum length λ_b is the separation at which the electrostatic interaction between two elementary charges is comparable in magnitude to the thermal energy scale. It is given by $\lambda_b = e^2 / 4\pi\epsilon_r\epsilon_0 k_b T = 7.16 \times 10^{-10}$ m for the fluids used in this work. Hence, all ions in

Table 2. Mean measured values from electrokinetic experiments.

Sample number	Grain diameter (laser) ($\times 10^{-6}$ m)	C_s $C_f = 2 \times 10^{-4}$ mol/L (V/MPa)	C_s $C_f = 2 \times 10^{-3}$ mol/L (V/MPa)	Calculated ζ $C_f = 2 \times 10^{-4}$ mol/L equation 4 (mV)	Calculated ζ $C_f = 2 \times 10^{-4}$ mol/L mol/L equation 6 (mV)	Calculated ζ $C_f = 2 \times 10^{-3}$ mol/L equation 4 (mV)	Calculated ζ $C_f = 2 \times 10^{-3}$ mol/L equation 6 (mV)
1	1.05	0.59	0.15	48.86	64.71	19.56	24.62
2	2.11	1.11	0.26	47.52	62.37	21.00	25.42
3	5.01	2.98	0.44	56.39	72.30	21.98	24.94
4	11.2	5.40	0.57	59.31	73.71	22.94	24.86
5	21.5	9.14	0.69	61.70	73.04	24.06	25.15
6	31.0	11.43	0.71	64.28	74.10	23.98	24.76
7	47.5	13.74	0.76	65.08	72.79	24.75	25.30
8	104	17.84	0.77	68.36	72.94	24.07	24.32
9	181	20.08	0.80	70.47	73.43	24.71	24.86
10	252	20.89	0.80	70.72	72.93	24.71	24.81
11	494	22.35	0.82	72.24	73.45	25.05	25.10
12	990	23.16	0.80	73.00	73.63	24.51	24.54
Mean				63.16	71.62	23.44	24.89

the bulk fluid and those in most of the diffuse layer are more affected by thermal perturbations than by other ions occupying the Stern layer. However, there is a thin mobile layer that is influenced greatly by the Stern layer ions.

The theoretical values of zeta potential arrived at in this work were 73.34 mV and 24.72 mV for fluid concentrations of $2 \times 10^{-4} \text{ mol L}^{-1}$ and $2 \times 10^{-3} \text{ mol L}^{-1}$, respectively. The zeta potential has also been calculated by inverting the streaming potential coupling coefficient measurements. The mean values of zeta potential are in fairly good agreement with the theoretical values as is described later in this paper.

Surface conductance. — This parameter was also calculated using the techniques described in [Revil and Glover \(1997\)](#) and in [Revil et al. \(1999b\)](#). The surface conductance is given in equations 18 by

$$\Sigma_s = \Sigma_s^{EDL} + \Sigma_s^{\text{Prot}} + \Sigma_s^{\text{Stern}} \quad (18)$$

where in equation 19

$$\Sigma_s^{\text{Stern}} = \frac{e\beta_s \Gamma_s^0 K_{Me} C_f}{\left(10^{-pH} + K_{(-)} \left(\frac{\sqrt{8 \times 10^{-3} \varepsilon_r \varepsilon_0 k_b T N}}{2e \Gamma_s^0 K_{(-)}} C^* \right)^{2/3} + K_{Me} C_f \right)} \quad (19)$$

where

$$C^* = \left((10^{-pH} + K_{Me} C_f) (C_a + C_f + 10^{-pH}) / \sqrt{\frac{1}{2} \sum_i Z_i^2 C_i^f} \right)$$

and where the contribution from the diffuse layer Σ_s^{EDL} was shown to be negligible by [Revil and Glover \(1998\)](#) and the contribution of the protons $\Sigma_s^{\text{Prot}} = 2.4 \times 10^{-9} \text{ S}$ ([Watillon and de Backer, 1970](#)). All the other parameters have already been described except β_s , which is the surface mobility (in $\text{m}^2 \text{ s}^{-1} \text{ V}^{-1}$). We have used $\beta_s = 5 \times 10^{-9} \text{ m}^2 \text{ s}^{-1} \text{ V}^{-1}$ from [Revil and Glover \(1998\)](#), and are not aware of any other reported values for this parameter. Detailed modeling work is presently being carried out, which indicates that varying this parameter within reasonable limits is not significant. The theoretical values of surface conduction arrived at in this work were $3.53 \times 10^{-9} \text{ S}$ and $4.49 \times 10^{-9} \text{ S}$ for fluid concentrations of $2 \times 10^{-4} \text{ mol L}^{-1}$ and $2 \times 10^{-3} \text{ mol L}^{-1}$, respectively. It was not possible to obtain experimental confirmation of the surface conductance because measurements were only carried out at two pore fluid salinities. However, the theoretical values calculated above are in good agreement with the determinations of other researchers ([Revil and Glover, 1997; 1998; Revil et al., 1999a; 1999b](#)). Since the surface conduction was not obtained experimentally, it was also not possible to confirm that the cementation exponent was constant at a value of $m = 1.5$, although this value is well accepted.

Hence, we have defined all the input parameters with respect to accepted theoretical values or experimental values that are relevant to our experimental system. The only true variable is the grain size and that is the functional variable.

The experimentally determined values of streaming potential coupling coefficient as a function of glass bead diameter are compared with the predictions of both the exact and approximate solutions of the theoretical equations in Figure 5 for both fluid concentrations. Curves are given in Figure 5 for various surface conductance values ($1 \times 10^{-10} \text{ S}$, $1 \times 10^{-9} \text{ S}$, and $1 \times 10^{-8} \text{ S}$) in order that the

sensitivity of the streaming coupling coefficient to this parameter may be judged. It is clear that the experimental determinations at both pore fluid concentrations verify the theoretical predictions very well. Providing we can trust the quality of the many input parameters needed for the theoretical models, it may be said that both the exact and approximate solutions fit the experimental data very well at the value of $\sigma_s = 3.53 \times 10^{-9} \text{ S}$, which is the value that arises from equation 18. For the low salinity data ($C_f = 2 \times 10^{-4} \text{ mol L}^{-1}$), the coefficients of determination are $R^2 = 0.984$ and $R^2 = 0.992$ for equation 4 and equation 6, respectively. For the high-salinity data ($C_f = 2 \times 10^{-3} \text{ mol L}^{-1}$) $R^2 = 0.855$ and $R^2 = 0.999$ for equation 4 and equation 6, respectively.

For some reason the approximate solution seems to fit the data marginally better than the exact solution of [Revil et al. \(1999a\)](#). However, it should be pointed out that a small change in some of the parameters is all that is required to enable the [Revil et al. \(1999a\)](#) model to fit the data just as well. For example, the [Revil et al. \(1999a\)](#) model fits the data for $C_f = 2 \times 10^{-4} \text{ mol/L}$ very well if the surface conductance is set equal to $5 \times 10^{-9} \text{ S}$ with all the other parameters kept constant. However, this represents a change of $+41\%$, and is greater than the surface conductance associated with a bulk solution 100 times more concentrated. Perhaps the uncertainties in some of the input parameters, such as the surface site density would make such a change possible; a surface site density of seven sites per nm^2 provides a surface conductance of $5.03 \times 10^{-9} \text{ S}$ and that is well within the range that some authors quote for quartz glass ([Iler, 1979](#)) though less than that previously used by [Revil et al. \(1999b\)](#). Unfortunately, small changes to this parameter such as this (and in $K_{(-)}$ and K_{Me}) cause the streaming potential coupling coefficient not to fit the experimental data in the large grain size limit (i.e., the classical HS limit). A more valid alternative method that allows equation 4 to fit the data better than that for equation 6 is to either increase the protonic surface conductivity contribution to $\Sigma_s^{\text{Prot}} = 3.4 \times 10^{-9} \text{ S}$, for both the low- and high-salinity data, or to disregard the statement by [Revil and Glover \(1998\)](#) that the EDL contribution is negligible, and set it to $\Sigma_s^{EDL} = 1 \times 10^{-9} \text{ S}$ for both the high- and low-salinity data. If this is carried out, the coefficients of determination for the models switch over and become $R^2 = 0.992$ and $R^2 = 0.985$ for equation 4 and equation 6, respectively for the low-salinity data, and $R^2 = 0.855$ and $R^2 = 0.906$ for equation 4 and equation 6, respectively for the high-salinity data.

Figure 5 shows (as in Figure 1) that at large grain sizes the measured streaming potential coupling coefficients approach that of the standard HS equation and decrease by about two orders of magnitude as the grain size reduces from about 1 mm to about 0.1 μm (23.16 V/MPa at 1 mm to $6.91 \times 10^{-2} \text{ V/MPa}$ at 0.1 μm for $C_f = 2 \times 10^{-4} \text{ mol/L}$ and 0.804 V/MPa at 1 mm to $1.79 \times 10^{-2} \text{ V/MPa}$ at 0.1 μm for $C_f = 2 \times 10^{-4} \text{ mol/L}$). It is very clear that, far from being a negligible secondary effect, the streaming potential coupling coefficient varies considerably with grain size. The new experimental data have demonstrated that both equation 4 and equation 6 are good models for describing the streaming potential coupling coefficient as a function of grain diameter.

Pore and pore throat size dependence

Figure 6 shows the same streaming potential coupling coefficient data, but this time as a function of the mean pore throat diameter of the glass bead pack. The pore throat diameter was obtained by mercury porosimetry of the bead packs while they were still in the sam-

ple tube in order not to disturb the relative position of the grains. The mean pore throat diameter was taken to be the modal value of a unimodal pore throat size distribution. The horizontal error bars in Figure 6 represent the half-height width of the pore throat size distribution.

It is clear in Figure 6 that equations 4 or 6 cannot be used to model the data because their input parameter is grain diameter whereas the data are plotted as a function of pore throat diameter ($R^2 = 0.760$ and $R^2 = 0.673$, respectively for the low-salinity data, and $R^2 = 0.4751$ and $R^2 = 0.4322$, respectively for the high-salinity data). The model curves plot to the right of the data because the grain diameter is larger than the pore throat diameter that was used to plot the experimental data (the offset can be calculated using equations 1 and 2 in Glover and Walker (2009)). There is also an offset between the experimental data and the model as a function of pore diameter (equation 10) because the pore diameter is larger than the pore throat diameter that was used to plot the data, although the offset is not as large because the pore diameter is only slightly larger than the pore throat diameter ($R^2 = 0.9522$ and 0.7667 for the low- and high-salinity data, respectively). This offset could be corrected for in the model by varying the value of a (to about 6.67 for Figure 6a, for example) or by changing the surface conductance (to 2×10^{-9} S in the case of Figure 6a). However, not only would such an ad hoc change cause the fit in Figure 5 to be much worse, values of a of such a size are not expected for bead packs or porous media (Glover et al., 2006). Figure 6 is an indicator of the size of the error that would follow from using the pore size, pore throat size, and grain size interchangeably.

As we have already said, the offset is actually due to the comparison of measurements as a function of pore throat diameter with a model that is a function of grain size (equations 4 and 6) or pore diameter (equations 9 and 10). Since pore throat diameter and pore diameter are not, in general, the same, we have modified equations 9 and 10 to generate a set of equations that are a function of pore throat diameter. In equations 20–22, we have used the following corrections

$$\text{For cubic packing } M_{\text{cubic}} = \frac{\sqrt{3} - 1}{\sqrt{2} - 1} = 1.7673. \quad (20)$$

$$\text{For random packing } M_{\text{rand}} = [1.655, 1.662]. \quad (21)$$

$$\text{For rhombohedral packing } M_{\text{rhom}} = \frac{3\sqrt{2} - 2\sqrt{3}}{4 - 2\sqrt{3}} = 1.4528. \quad (22)$$

Here M is the ratio of the pore size radius (or diameter) to the pore throat radius (or diameter). These relationships are derived in the Appendix. The cubic and rhombohedral packing represent the end members for contacting nonbroken spheres of uniform size. The random packing is expected to lie between these values but is not tractable analytically. The two values given by equation 21 represent the results of linear and quadratic interpolations for random packing with equations $M = 1.642\phi + 1$ ($R^2 = 0.9967$), which gives $M_{\text{rand}} = 1.655$, and $M = -0.6324\phi^2 + 1.918\phi + 1$ ($R^2 = 1.000$), which gives $M_{\text{rand}} = 1.662$, where ϕ is the porosity of the structure, and it has been assumed that compaction due to rearrangement of the struc-

ture of the porous media causes monotonic changes in the porosity, pore throat diameter, and pore size. In reality, this process must be regarded as an approximation as the mathematical description of sphere packing is very complex. It is not possible to add further unique points to the figure in Appendix A because all other regular packing structures have multiple pore and/or pore throat sizes.

If we use equations 20–22 to transform the pore radii values in equations 9 and 10 into pore throat diameters, in equations 23, through 26, we get:

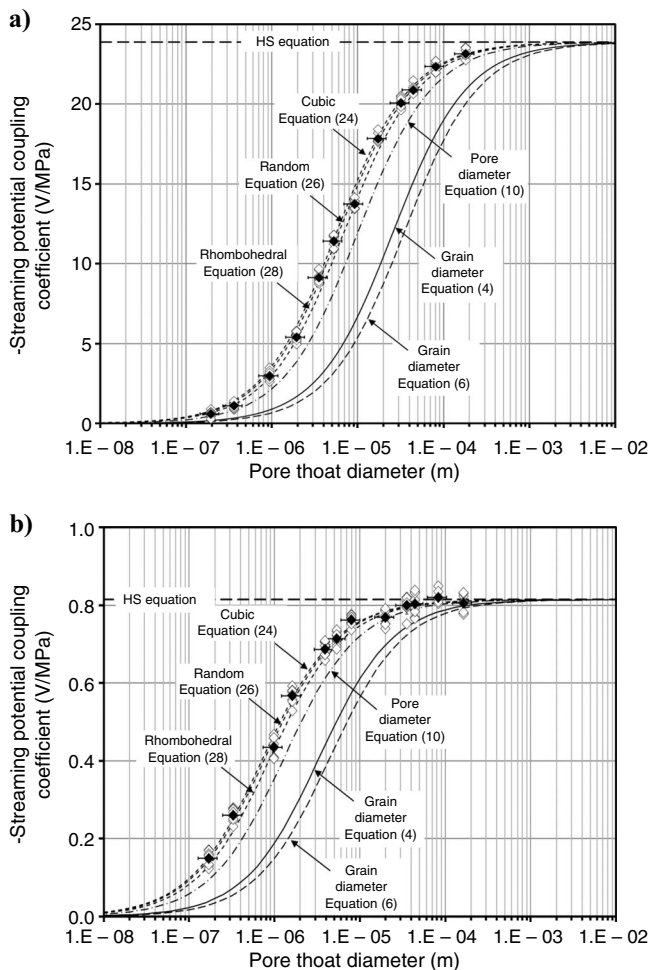


Figure 6. Streaming potential coupling coefficients of a range of quartz glass bead packs as a function of the mean pore throat diameter of the glass bead pack. (a) Pore fluid salinity $C_f = 2 \times 10^{-4}$ mol/L, (b) Pore fluid salinity $C_f = 2 \times 10^{-3}$ mol/L. The open symbols show the streaming potential coupling coefficient measurements for individual flow rates at a given grain size, which shows their uncertainty. The solid symbols show the calculated mean value. The horizontal error bar shows the effective standard deviation of the laser diffraction bead size measurements. The long dashed line is the result assuming falsely that the grain diameter equation (equation 6) can be used to predict the variability of the streaming potential coupling coefficient as a function of pore throat size. Likewise, the solid line is the result assuming, again falsely, that the pore diameter equation (equation 10) can be used. The short dashed lines are the results of using the pore throat diameter equations, with curves for cubic, random, and rhombohedral packing (equations 24, 26, and 28, respectively).

For cubic packing C_s

$$= \frac{d_{PT}\varepsilon_f\zeta\sqrt{a}(\sqrt{3}-1)}{\eta_f(d_{PT}\sqrt{a}(\sqrt{3}-1)\sigma_f + 8\Sigma_s\sqrt{2}(\sqrt{2}-1))} \text{ in general} \quad (23)$$

and

$$C_s = \frac{d_{PT}\varepsilon_f\zeta(\sqrt{3}-1)}{\eta_f(d_{PT}(\sqrt{3}-1)\sigma_f + 4\Sigma_s\sqrt{3}(\sqrt{2}-1))} \text{ for } a = 8/3. \quad (24)$$

For random packing C_s

$$= \frac{d_{PT}M_{\text{rand}}\varepsilon_f\zeta\sqrt{a}}{\eta_f(d_{PT}M_{\text{rand}}\sqrt{a}\sigma_f + 8\Sigma_s\sqrt{2})} \text{ in general} \quad (25)$$

and

$$C_s = \frac{d_{PT}M_{\text{rand}}\varepsilon_f\zeta}{\eta_f(d_{PT}M_{\text{rand}}\sigma_f + 4\Sigma_s\sqrt{3})} \text{ for } a = 8/3. \quad (26)$$

In equations 27 and 28, for rhombohedral packing

$$C_s = \frac{d_{PT}\varepsilon_f\zeta\sqrt{a}(3\sqrt{2}-2\sqrt{3})}{\eta_f(d_{PT}\sqrt{a}(3\sqrt{2}-2\sqrt{3})\sigma_f + 8\Sigma_s\sqrt{2}(4-2\sqrt{3}))} \text{ in general} \quad (27)$$

and

$$C_s = \frac{d_{PT}\varepsilon_f\zeta(3\sqrt{2}-2\sqrt{3})}{\eta_f(d_{PT}(3\sqrt{2}-2\sqrt{3})\sigma_f + 4\Sigma_s\sqrt{3}(4-2\sqrt{3}))} \text{ for } a = 8/3. \quad (28)$$

These equations have been deliberately left in a form that is not quite their simplest in order that their shared structure can be compared. The general form is seen in equation 29

$$C_s = \frac{d_{PT}M_i\varepsilon_f\zeta\sqrt{a}}{\eta_f(d_{PT}M_i\sqrt{a}\sigma_f + 8\Sigma_s\sqrt{2})} \quad (29)$$

for any shape of grain, where M_i is the relevant pore size to pore throat ratio for the style of packing present, and in equation 30

$$C_s = \frac{d_{PT}M_i\varepsilon_f\zeta}{\eta_f(d_{PT}M_i\sigma_f + 4\Sigma_s\sqrt{3})} \quad (30)$$

for the special case of monodisperse spheres, where $a = 8/3$.

Figure 6 shows that all the models as a function of pore throat diameter match the experimental data very well. It seems that the random packing model fits the data slightly better than the cubic or rhombohedral models, which fall to either side of it. For the low-salinity data ($C_f = 2 \times 10^{-4}$ mol L⁻¹), the coefficients of determination are $R^2 = 0.9777$, 0.9784 and 0.9770 for cubic, random, and rhombohedral packing (equations 24, 26, and 28), respectively. For the high-salinity data ($C_f = 2 \times 10^{-3}$ mol L⁻¹), $R^2 = 0.9771$, 0.9935 , and 0.9303 for cubic, random, and rhombohedral packing (equations 24, 26, and 28), respectively.

This supposition has not been checked statistically because the range of values expressed by the three models falls within the range of uncertainties in the experimental data, and hence, the power of a formal statistical test would be small. Providing the appropriate model is used, it may be said that the experimental data are predicted well by the equations for the streaming potential coupling coefficient as a function of pore throat size.

The x -offset of each of the curves (cubic, random, rhombohedral) with respect to that for the grain diameter can be expressed in terms of the d_{PT}/d ratio. This ratio takes the values 0.4142, 0.1757, and 0.1547 for the cubic, random, rhombohedral structures, respectively. The ratio can be calculated from the experimental data and is found to be equal to 0.1807. It is clear that the experimental values agree very well with the theoretical predictions.

ZETA POTENTIAL

We have noted that the theoretical model for the streaming potential coupling coefficient as a function of grain diameter (equations 4 and 6) seems to fit the data very well. The question arises whether the inverse calculation of the zeta potential from the experimental data using these equations would provide a constant zeta potential, i.e., one that is not a function of grain size, pore size, or flow rate. Such a result would agree well with previously described forward models that calculate zeta potential from electro-chemical considerations (Revil and Glover, 1997; Revil et al., 1999a) (i.e., equations 15–17) because these forward models do not explicitly consider grain size, pore size, pore throat size or fluid flow.

We have carried out this process to examine the change in zeta potential implied by the exact and approximate solutions (equations 4 and 6, respectively). In these calculations, we have kept all the other parameters the same as in the forward model. The results of the calculations are shown in Table 2.

The mean zeta potentials (all flow rates and grain sizes) from the exact solution from the Revil et al. (1999a) model (equation 4) were 63.13 ± 9.87 mV for a bulk fluid concentration of 2×10^{-4} mol/L and 23.44 ± 1.95 mV for a bulk fluid concentration of 2×10^{-4} mol/L. The corresponding values for the approximate solution of Glover et al. (2006) (equation 6) were 71.62 ± 7.76 mV for a bulk fluid concentration of 2×10^{-4} mol/L and 24.89 ± 1.21 mV for a bulk fluid concentration of 2×10^{-4} mol/L. The theoretically calculated values that were used in the forward modeling (from equations 15–17) were 73.34 mV for $C_f = 2 \times 10^{-4}$ mol/L and 24.72 mV for $C_f = 2 \times 10^{-3}$ mol/L.

Formal statistical analysis shows that there is no significant difference between the results of either the exact solution and the theoretically modeled values ($p = 0.306$ and $p = 0.515$, for $C_f = 2 \times 10^{-4}$ mol/L, and $C_f = 2 \times 10^{-3}$ mol/L, respectively) or the approximate solution and the theoretically modeled values ($p = 0.826$ and $p = 0.889$, for $C_f = 2 \times 10^{-4}$ mol/L, and $C_f = 2 \times 10^{-3}$ mol/L, respectively). Here the p -value is the probability of obtaining a test statistic at least as extreme as the one that was actually observed, assuming that the null hypothesis is true. Hence, there is fairly good general agreement between the theoretical values and the values from either the exact or approximate solutions to the streaming potential coupling coefficient grain size.

Parts (a) and (b) of Figure 7 show the calculated zeta potential obtained by inverting equations 4 and 6 as a function of grain size for $C_f = 2 \times 10^{-4}$ mol/L NaCl and $C_f = 2 \times 10^{-3}$ mol/L NaCl, respectively. The mean zeta potential calculated from equation 6 does

not change significantly with grain size. The vertical error bars represent ± 1 standard deviation in the values calculated from measurements made for individual flow rates and directions. It is clear that there is an increase in the scatter of the individual measurements at small grain sizes. This is due to larger fractional experimental errors for smaller grain sizes that have low streaming potentials that are difficult to measure accurately. The scatter in individual measurements also increases at low grain sizes for zeta potentials calculated using equation 4; however, there is also a systematic decrease in zeta potential with decreasing grain size. This decrease can also be generated by adjusting the surface conductance in equation 6 so that it becomes $F/(F - 1)$ larger, i.e., to render the approximate solution into the exact solution. The data indicate, therefore, that either the zeta potential itself diminishes slightly with grain size or the model is not yet complete.

Parts (c) and (d) of Figure 7 show the calculated zeta potential as a function of flow rate for the individual measurements. The scatter in the individual measurements increases as the flow rate decreases for both the exact and the approximate solutions due to the difficulty in measuring small streaming potentials associated with small flow rates. The general trend for the data from the approximate solution is constant, although there may be a small reduction in the zeta poten-

tials obtained from the exact solution of Revil et al. (1999a), which begs the question whether the streaming potential is fully developed at low flow rates during viscous flow.

This work indicates that there may be a dependence of the zeta potential on grain size and flow rate for smooth quartz glass beads saturated with NaCl solutions between $C_f = 2 \times 10^{-4}$ and $C_f = 2 \times 10^{-3}$ mol/L. If this is so, there may also be a dependence for non-spherical or rough glass beads, for polydisperse beads, and for real rocks. Recently, in an excellent study, Leroy et al. (2008) have found the roughness of glass beads to have an important effect on the modeled and experimental values of the complex conductivity of bead packs; it may also be true that the zeta potential depends on a greater range of parameters than was originally thought.

CONCLUSIONS

We have examined the effect of varying grain size, pore size, and pore throat size on the streaming potential coupling coefficient of porous granular media both theoretically and experimentally.

We have compared the classical HS model with the grain size-dependent model of Revil in its exact form and in the approximate form derived from Glover et al., and also with two previously existing data sets. This comparison shows the classical HS model to be insufficient to describe granular porous media. It also shows that the grain diameter-dependent model works very well in either its exact form, $R^2 = 0.926$ or its approximate form, $R^2 = 0.890$.

We have also developed a streaming potential coupling coefficient relationship that is a function of mean pore radius using the findings of Glover and Walker. This new relationship provides the opportunity to calculate the streaming potential coupling coefficient from pore size data, which is a routine measurement made using image analysis and can also be obtained from permeability measurements on rocks.

We have carried out streaming potential coupling coefficient measurements on a suite of 12 monodisperse quartz glass bead packs each with a different well-characterized grain size, and for two different pore fluid salinities. These glass bead packs have a large range of permeability, so special methods were developed to measure small streaming potentials and pressure differences with sufficient accuracy. The experimental results provide a much better test of the theoretical models than the earlier data, showing that the shape of the streaming potential coupling coefficient curves is correct over a large range of grain and pore sizes. Forward modeling with no adjustable parameters has shown that the grain diameter-dependent model in either its exact form ($R^2 = 0.984$ and $R^2 = 0.855$ for $C_f = 2 \times 10^{-4}$ mol/L and $C_f = 2 \times 10^{-3}$ mol/L NaCl, respectively) or its approximate form ($R^2 = 0.992$ and $R^2 = 0.999$ for $C_f = 2 \times 10^{-4}$ mol/L and $C_f = 2 \times 10^{-3}$ mol/L NaCl, respectively) describe the new data very well. The difference between the exact and approxi-

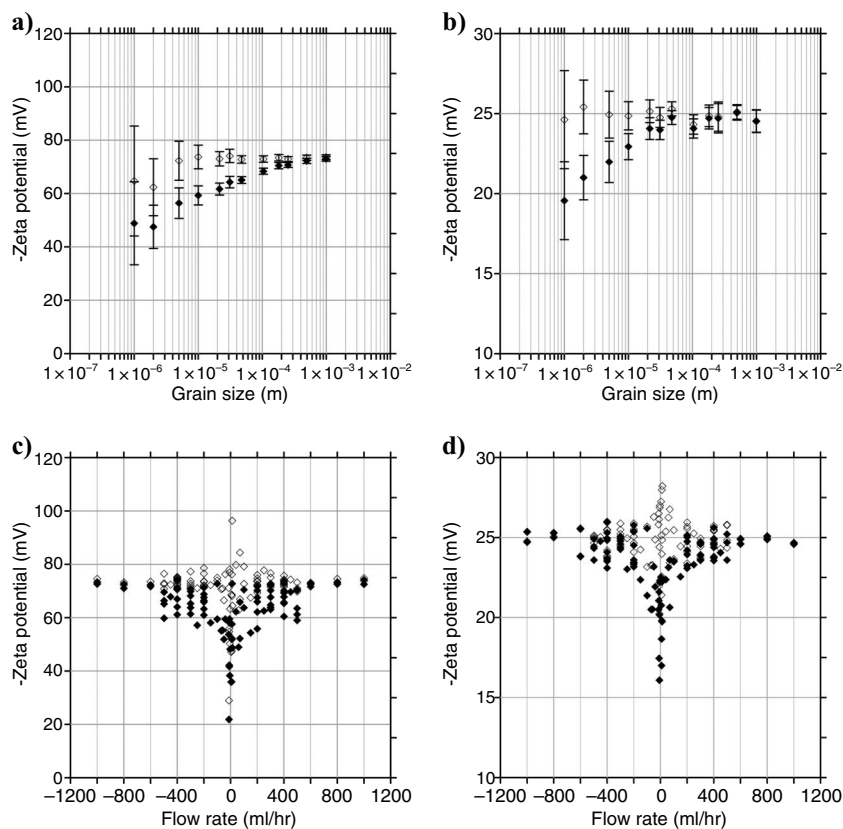


Figure 7. Calculated values of the zeta potential obtained from inversion using equation 4 and equation 6 together with the measured streaming potential coupling coefficient as a function of grain size. Parts (a) and (b) show the inverted zeta potential as a function of grain diameter; parts (c) and (d) show them as a function of fluid flow rate, for fluid concentrations of $C_f = 2 \times 10^{-4}$ mol/L and $C_f = 2 \times 10^{-3}$ mol/L, respectively. In parts (a) and (b), the solid symbols and open symbols represent the zeta potentials as a function of grain size (irrespective of flow rate) using equation 4 and 6 respectively, while the error bars show the variation in the data caused by using different flow rates (± 1 standard deviation). In parts (c) and (d), the solid symbols represent the inverted zeta potentials using equation 4, while the open triangles represent those obtained using equation 6.

mate solutions is small despite the formation factor for glass beads being $F \approx 4$, which does not fulfill the criterion that $F \gg 1$, and may be taken account of by small changes in the values of some input parameters. The difference would be truly negligible for real rocks where F commonly varies between 10 and 100. Consequentially, we can confirm that either the exact form of the streaming potential coupling coefficient grain size relationship or its approximate form can be used to calculate the streaming potential coupling coefficient of reservoir rocks as a function of grain size.

Experimental measurements were also carried out to test newly developed relationships between streaming potential coupling coefficient and mean pore radius (equations 9 and 10), and it was found that the relationships behaved very well. By consequence we can confirm that equations 9 and 10 can be used to calculate the streaming potential coupling coefficient of reservoir rocks as a function of pore size.

A comparison of the measured streaming potential coupling coefficient data as a function of the modal pore throat size showed an offset between the results of equation 10 because this equation was created for a mean pore radius not a mean pore throat diameter. We analyzed the geometric difference between these two values and corrected the model to be valid for cubic, rhombohedral, and random packings (equations 23–30). It was then found that while the random packing model provided the best fit to the data ($R^2 = 0.9784$ and 0.9834 for $C_f = 2 \times 10^{-4}$ mol/L and $C_f = 2 \times 10^{-3}$ mol/L NaCl, respectively), the cubic and rhombohedral packing models also fit the data within its uncertainties (for the low-salinity data $R^2 = 0.9777$ and 0.9770 and for the high-salinity data $R^2 = 0.9771$ and 0.9303 both for cubic and rhombohedral packing, respectively). In consequence, we can confirm that equations 29 and 30 with $M_i = 1.662$ can be used to calculate the streaming potential coupling coefficient of reservoir rocks as a function of pore throat diameter.

Finally, the zeta potential was calculated from the new streaming potential coupling coefficient data using the exact form of the streaming potential coupling coefficient grain size relationship and its approximate form. In all cases, the calculated zeta potentials were in reasonable agreement with those calculated from the theory of Revil and Glover ($P \leq 0.306$).

It should be noted that the sensitivity of the streaming potential coupling coefficient to grain size arises from the surface conduction term in the HS equation. The consequence is that a dependence on grain size (pore size and pore throat size) may be noted only for rocks saturated with low-salinity fluids, where the surface conductivity plays a significant role. Brines are very saline in most hydrocarbon reservoirs ($C_f > 1$ mol/L), and therefore, the surface conductivity is negligible.

This paper has presented new streaming potential data as a function of grain size to a literature that was all but lacking in such data. This is important because electrokinetic measurements are beginning to be used in many aspects of reservoir engineering and one of the most common ways of describing a reservoir rock is by its grain size, pore size, and pore throat size. The relationships between the streaming potential coupling coefficient of a rock and its mean grain size, pore size, or pore throat size, that have been either cited or developed in this work, are useful tools for predicting the streaming potential coupling coefficients likely to be developed in water and hydrocarbon reservoirs with low salinities. Those with high salinities will not be sensitive to grain size changes. It should also be noted that it has been observed that fractured natural materials, such as Westerly granite, tend to have streaming potential coupling coefficients that

are less than those obtained for measurements on glass beads and capillary tubes. Hence, we cannot exclude the operation of textural effects other than grain size.

ACKNOWLEDGMENTS

This work has been made possible thanks to funding by the Natural Sciences and Engineering Research Council of Canada (NSERC) Discovery Grant Programme. We would also like to thank the assistant editor, Evert Slob; the associate editor, Phil Benson; Alexis Mainault, and five other anonymous reviewers for their constructive comments, modifications, and additions, which have substantially improved the manuscript.

APPENDIX A

The following calculations assume that the pore diameter and pore throat diameter are represented by the diameter of the largest sphere that may fit inside a structure made from spherical beads (which we call the diameter of occupation), or may pass into the said structure through an opening (which we call the diameter of entrance).

The densest packing of nonbroken single-sized spheres in contact is rhombohedral, and the least dense is cubic. We take these two structures as limits, noting that each has a well-defined and unique diameter of occupation and diameter of entry. In each case, we quote or derive (1) the porosity of the structure, (2) the ratio of the pore diameter (diameter of occupation) to the grain diameter, (3) the ratio of the pore throat diameter (diameter of entrance) to the grain diameter, and (4) the ratio of the pore diameter to the pore throat diameter.

For cubic unit cell composed of spheres of diameter d the pore diameter d_p is given by equation A-1

$$d_p = d(\sqrt{3} - 1) = 0.7320d \quad (\text{A-1})$$

and the pore throat diameter d_{pT} is given in equation A-2

$$d_{pT} = d(\sqrt{2} - 1) = 0.4142d. \quad (\text{A-2})$$

Hence, the ratio of the pore size to the pore throat size is independent of d and given in equation A-3 by

$$M_{cubic} = \frac{d_p}{d_{pT}} = \frac{\sqrt{3} - 1}{\sqrt{2} - 1} = 1.7673. \quad (\text{A-3})$$

Because the volume of the unit cell is $8d^3$ and the cell contains one sphere (eight-eighths of a sphere each centered at each corner of the unit cell), the porosity can be easily calculated in equation A-4 to be

$$\phi = 1 - \frac{\pi}{6} = 0.4764. \quad (\text{A-4})$$

For the rhombohedral structure unit cell, the derivation of the values is more complex.

The pore diameter d_p is given in equation A-5 by

$$d_p = d\left(\frac{\sqrt{6}}{2} - 1\right) = 0.2247d, \quad (\text{A-5})$$

which can be found by calculating the length of the line from any vertex to the centroid of the opposite face. This length is effectively the “height” of the tetrahedron. The centroid of the tetrahedron falls

on this line in the ratio 3:1 from the vertex. Hence, one can calculate the distance from the vertex to the centroid of the tetrahedron, say b . The radius of the largest sphere that can fit inside the packing is b minus the radius of the rhombohedrally arranged spheres (i.e., $d/2$). The value calculated in equation A-5 is consistent with the critical ratio of occupation value quoted by Yang (2003). The critical ratio of occupation is the ratio of the diameter of the matrix spheres to that of the largest sphere that will fit within the structure and, for the rhombohedral structure, is given by $d/d_p = 4.444$ (Cumberland and Crawford, 1987).

The pore throat diameter d_{PT} is

$$d_{PT} = d \left(\frac{2}{\sqrt{3}} - 1 \right) = 0.1547d, \quad (\text{A-6})$$

which can be found simply by calculating the length of the line on any face from any vertex to the centroid of that face and then subtracting the sphere radius from the result. The value calculated in equation A-6 is consistent with the critical ratio of entrance value quoted by Yang (2003). The critical ratio of entrance is the ratio of the diameter of the matrix spheres to that of the largest sphere that can enter the structure and, for the rhombohedral structure, is given $d/d_{PT} = 6.464$ (Cumberland and Crawford, 1987).

Hence, the ratio of the pore size to the pore throat size is independent of d and in equation A-7 given by

$$M_{\text{rhom}} = \frac{d_p}{d_{PT}} = \frac{3\sqrt{2} - 2\sqrt{3}}{4 - 2\sqrt{3}} = 1.4528. \quad (\text{A-7})$$

Because the volume of the unit cell is $\sqrt{2}d^3/12$ and the cell contains 1/6 of a sphere (4/24 of a sphere each centered at each corner of the unit cell), the porosity of the rhombohedral sphere packing can be easily calculated in equation A-8 to be

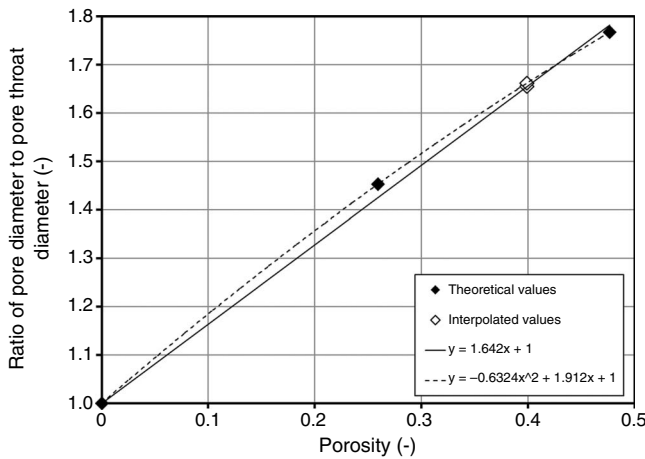


Figure A-1. The calculated pore diameter to pore throat diameter ratio as a function of calculated porosity. The three solid symbols indicate the points $(\phi = 0, M = 1)$, $(0.4764, 1.767)$, $(0.2595, 1.453)$, which represent a theoretical limit, the rhombohedral structure, and the cubic structure, respectively. The open symbols (almost co-located) represent the results of linear and quadratic interpolation for random packing with equations $M = 1.642\phi + 1$ ($R^2 = 0.997$) and $M = -0.6324\phi^2 + 1.912\phi + 1$ ($R^2 \approx 1.000$), shown as solid and dashed lines, respectively.

$$\phi = 1 - \frac{\pi\sqrt{2}}{6} = 0.2595. \quad (\text{A-8})$$

It is possible to use the relationships between pore size and pore throat size for the cubic and rhombohedral structures given by equations A-3 and A-7 together with equations 9 and 10 to produce equations that describe the streaming potential coupling coefficient of a porous medium as a function of its pore throat size for each structure. This has been carried out. Equations 23 and 24 are valid for a cubic structure; equations 27 and 28 are valid for the rhombohedral structure. These are limiting cases.

Neither real rocks nor the bead packs used in our experimental measurements have cubic or rhombohedral structures; their beads and grains are arranged randomly. We can, however, approximate an equation for the pore diameter to pore throat diameter ratio for a random distribution of monodisperse beads in the following manner. The difference between the cubic and rhombohedral packing represents the range of possible compaction possible if the beads are spherical, of the same diameter, not broken, and in contact. Bearing these constraints in mind, compaction alters the structure incrementally during which there is (1) a reduction in the mean pore diameter, (2) a reduction in the mean pore throat diameter, and (3) a reduction in the porosity. During the change from a low-density packing that is represented by the cubic structure, to the densest packing that is represented by the rhombohedral structure, the system will pass through a structure that best represents a random distribution. Depending on the magnitudes of the reductions in pore diameter and mean pore throat diameter during this change, their ratio will also change. Because we have the value of the ratio M and porosity ϕ for each of the extreme positions and the porosity for the random packing, $\phi = 0.399$ (Wyllie and Gregory, 1955; Guéguen and Palciauskas, 1994), it is possible to calculate the ratio for the random structure by interpolation. Figure A-1 shows such an interpolation graphically. There are three fixed points that are not quite co-linear $(\phi = 0, M = 1)$, $(0.4764, 1.767)$, $(0.259, 1.453)$. The linear interpolation between these three points was $M = 1.642\phi + 1$ (with the fitting parameter $R^2 = 0.9967$), which gives a value of $M_{\text{random}} = 1.655$. We also carried out a quadratic fitting and obtained $M = -0.6324\phi^2 + 1.912\phi + 1$ (with the fit parameter being fixed at $R^2 \approx 1.000$ because only three points are used to define the curve). The quadratic fit gives a value of $M_{\text{random}} = 1.662$. The difference between the two fits is 2.24% of the difference between the values of M obtained from the cubic and rhombohedral end members. Hence, for a random packing of single-sized spheres, the pore diameter is approximately 1.66 times the size of the pore throat diameter. The fitted values can then be used to develop equations that describe the streaming potential coupling coefficient of a porous medium as a function of its pore throat size for a random arrangement of grains or beads, which are given as equations 25 and 26.

Please note that the pore diameters calculated for the two regular lattices (i.e., equations A-2 and A-6) are absolute measures of the pore diameter of occupation, whereas the pore diameter implied by equation 7 and used in equations 9 and 10 is an effective value that is valid for any pore and grain structure, and that is derived from electrokinetic considerations that do not require the assumption of a capillary tube (Glover and Walker, 2009). The only place in this paper where the three measures are used at the same time, and hence, where a compatibility problem might arise, is in Figure A-1. However, here we carry out two empirical fits which take account of the change between the absolute measures given by equations A-2 and

A-6 and the effective value required by equations 9 and 10. Hence, the interpolated values of M that arise from the fittings in Figure A-1 are compatible with equations 9 and 10, which imply that equations 25 and 26 are compatible with those for the regular lattices.

REFERENCES

- Ahmad, M. U., 1964, A laboratory study of streaming potentials Geophysical Prospecting, **12**, no. 1, 49–64, doi: 10.1111/j.1365-2478.1964.tb01889.x.
- Archie, G. E., 1942, The electrical resistivity log as an aid in determining some reservoir characteristics: Transactions of the American Institute of Mining, Metallurgical, and Petroleum Engineers (AIME), **146**, 54–67.
- Bolève, A., A. Crespy, A. Revil, F. Janod, and J. L. Mattiuzzo, 2007, Streaming potentials of granular media: Influence of the Dukhin and Reynolds numbers: Journal of Geophysical Research, **112**, B8, B08204, doi: 10.1029/2006JB004673.
- Booth, F., 1951, The dielectric constant of water and the saturation effect: The Journal of Chemical Physics, **19**, no. 4, 391–394, doi: 10.1063/1.1748233.
- Bull, H. B., and R. A. Gortner, 1932, Electrokinetic potentials. X. The effect of particle size on the potential: Journal of Physical Chemistry, **36**, no. 1, 111–119, doi: 10.1021/j150331a007.
- Cumberland, D. J., and R. J. Crawford, 1987, The packing of particles: handbook of powder technology, 6: Elsevier.
- Dupuis, J., K. Butler, A. Keping, and B. Harris, 2009, Anatomy of a seismic-electric conversion: Measurements and conceptual modeling in boreholes penetrating a sandy aquifer: Journal of Geophysical Research, doi: 10.1029/2008JB005939.
- Glover, P. W. J., and M. D. Jackson, 2010, Borehole electrokinetics: The Leading Edge, **29**, no. 6, 724–728, doi: 10.1190/1.3447786.
- Glover, P. W. J., and E. Walker, 2009, Grain size to effective pore size transformation derived from an electro-kinetic theory: Geophysics, **74**, no. 1, E17–E29, doi: 10.1190/1.3033217.
- Glover, P. W. J., I. I. Zadjali, and K. A. Frew, 2006, Permeability prediction from MICP and NMR data using an electrokinetic approach: Geophysics, **71**, no. 4, F49–F60, doi: 10.1190/1.2216930.
- Grahame, D. C., 1947, The electrical double layer and the theory of electrocapillarity: Chemical Reviews, **41**, no. 3, 441–501, doi: 10.1021/cr60130a002.
- , 1950, Effects of dielectric saturation upon the diffuse double layer and free energy of hydration of ions: The Journal of Chemical Physics, **18**, no. 7, 903–909, doi: 10.1063/1.1747807.
- Guéguen, Y., and V. Palciauskas, 1994, Introduction to the physics of rocks: Princeton University Press.
- Guichet, X., and P. Zuddas, 2003, Effect of secondary minerals on electrokinetic phenomena during water-rock interaction: Geophysical Research Letters, **30**, no. 13, 1714–1718, doi: 10.1029/2003GL017480.
- Hiemstra, T., J. C. M. De Wit, and W. H. Van Riemsdijk, 1989a, Multisite proton adsorption modeling at the solid/solution interface of (hydr)oxides: A new approach. II. Application to various important (hydr)oxides: Journal of Colloid and Interface Science, **133**, no. 1, 105–117, doi: 10.1016/0021-9797(89)90285-3.
- Hiemstra, T., W. H. Van Riemsdijk, and G. H. Bolt, 1989b, Multisite proton adsorption modeling at the solid/solution interface of (hydr)oxides: A new approach. I. Model description and evaluation of intrinsic reaction constants: Journal of Colloid and Interface Science, **133**, no. 1, 91–104, doi: 10.1016/0021-9797(89)90284-1.
- Hunter, R. J., 1966, The interpretation of electrokinetic potentials: Journal of Colloid and Interface Science, **22**, no. 3, 231–239, doi: 10.1016/0021-9797(66)90028-2.
- Hunter, R. L., 1981, Zeta potential in colloidal science: Academic Press.
- Iglesias, T. P., and J. Péon Fernández, 2001, A mixing rule for the permittivity of binary mixtures in a framework of a weak-fluctuations model: Journal of Materials Science Letters, **20**, no. 14, 1333–1334, doi: 10.1023/A:1010962920679.
- Iler, R. K., 1979, The Chemistry of Silica: Wiley.
- Ishido, T., and H. Mizutani, 1981, Experimental and theoretical basis of electrokinetic phenomena to rock-water systems and its application to geophysics: Journal of Geophysical Research, **86**, B3, 1763–1775, doi: 10.1029/JB086iB03p01763.
- Jaafar, M., J. Vinogradov, and M. Jackson, 2009, Measurement of streaming potential coupling coefficient in sandstones saturated with high salinity NaCl brine: Geophysical Research Letters, **36**, L21306, doi: 10.1029/2009GL040549.
- Joergensen, S. S., and A. Tovberg-Jensen, 1967, Acid-base properties of quartz suspensions: Journal of Physical Chemistry, **71**, no. 3, 745–750, doi: 10.1021/j100862a040.
- Jouniaux, L., and J.-P. Pozzi, 1995a, Permeability dependence of streaming potential in rocks for various fluid conductivities: Geophysical Research Letters, **22**, no. 4, 485–488, doi: 10.1029/94GL03307.
- , 1995b, Streaming potential and permeability of saturated sandstones under triaxial stress: Consequences for electrotelluric anomalies prior to earthquakes: Journal of Geophysical Research, **100**, B6, 10197–10209, doi: 10.1029/95JB00069.
- Kuwano, O., M. Nakatani, and S. Yoshida, 2006, Effect of the flow state on streaming current: Geophysical Research Letters, **33**, no. 21, L21309, doi: 10.1029/2006GL027712.
- Leroy, P., and A. Revil, 2004, A triple-layer model of the surface electrochemical properties of clay minerals: Journal of Colloid and Interface Science, **270**, no. 2, 371–380, doi: 10.1016/j.jcis.2003.08.007.
- Leroy, P., A. Kemna, P. Cosenza, and A. Ghorbani, 2008, Complex conductivity of water-saturated packs of glass beads: Journal of Colloid and Interface Science, **321**, no. 1, 103–117, doi: 10.1016/j.jcis.2007.12.031.
- Li, S. X., D. B. Pengra, and P. Wong, 1995, Onsager's reciprocal relation and the hydraulic permeability of porous media: Physical Review E: Statistical Physics, Plasmas, Fluids, and Related Interdisciplinary Topics, **51**, no. 6, 5748–5751, doi: 10.1103/PhysRevE.51.5748.
- Lide, D. R., 2009, Handbook of chemistry and physics, 90th edition: CRC Press.
- Lorne, B., F. Perrier, and J.-P. Avouac, 1999, Streaming potential measurements. I. Properties of the electrical double layer from crushed rock samples: Journal of Geophysical Research, **104**, B8, 17857–17877, doi: 10.1029/1999JB900156.
- Lyklema, J., and J. T. G. Overbeek, 1961, On the interpretation of electrokinetic potentials: Journal of Colloid and Interface Science, **16**, 501–512, doi: 10.1016/0095-8522(61)90029-0.
- Maineult, A., Y. Bernabé, and P. Ackerer, 2004, Electrical response of flow, diffusion, and advection in a laboratory sand box: Vadose Zone Journal, **3**, no. 4, 1180–1192, doi: 10.2113/3.4.1180.
- Morgan, F. D., E. R. Williams, and T. R. Madden, 1989, Streaming potential properties of Westerly Granite with applications: Journal of Geophysical Research, **94**, B9, 12449–12461, doi: 10.1029/JB094iB09p12449.
- Ogilvy, A. A., M. A. Ayed, and V. A. Bogoslovsky, 1969, Geophysical studies of water leakages from reservoirs: Geophysical Prospecting, **17**, no. 1, 36–62, doi: 10.1111/j.1365-2478.1969.tb02071.x.
- Overbeek, J. T. G., 1952, Electrochemistry of the double layer: in H. R. Kruyt, ed., Colloid Science, **1**, 115–193, Elsevier.
- Phillips, S. L., H. Ozbek, and R. J. Otto, 1978, Basic energy properties of electrolytic solutions database: Sixth International CODATA Conference Santa Flavia (Palermo), Sicily, Italy, May 22–25, accessed 10 June 2010, <http://www.osti.gov/bridge/purl.cover.jsp;jsessionid=3954E775156A8BC0FA35DB5CE5B402D4?pu=6269880-iP-JPhB/>.
- Pride, S., 1994, Governing equations for the coupled electro-magnetics and acoustics of porous media: Physical Review B: Condensed Matter and Materials Physics, **50**, no. 21, 15678–15696, doi: 10.1103/PhysRevB.50.15678.
- Pride, S., and F. D. Morgan, 1991, Electrokinetic dissipation induced by seismic waves: Geophysics, **56**, no. 7, 914–925, doi: 10.1190/1.1443125.
- Revil, A., 2002, The hydroelectric problem of porous rocks: thermodynamic approach and introduction of a percolation threshold: Geophysical Journal International, **151**, no. 3, 944–949, doi: 10.1046/j.1365-246X.2002.01815.x.
- Revil, A., and L. M. Cathles III, 1999, Permeability of shaly sands: Water Resources Research, **35**, no. 3, 651–662, doi: 10.1029/98WR02700.
- Revil, A., and P. W. J. Glover, 1997, Theory of ionic surface electrical conduction in porous media: Physical Review B: Condensed Matter and Materials Physics, **55**, no. 3, 1757–1773, doi: 10.1103/PhysRevB.55.1757.
- , 1998, Nature of surface electrical conductivity in natural sands, sandstones, and clays: Geophysical Research Letters, **25**, no. 5, 691–694, doi: 10.1029/98GL00296.
- Revil, A., P. A. Pezard, and P. W. J. Glover, 1999a, Streaming potential in porous media 1. Theory of the zeta potential: Journal of Geophysical Research, **104**, B9, 20021–20031, doi: 10.1029/1999JB900089.
- Revil, A., H. Schwaeger, L. M. Cathles III, and P. D. Manhardt, 1999b, Streaming potential in porous media 2. Theory and application to geothermal systems: Journal of Geophysical Research, **104**, B9, 20033–20048, doi: 10.1029/1999JB900090.
- Saunders, J. H., M. D. Jackson, and C. C. Pain, 2008, Fluid flow monitoring in oil fields using downhole measurements of electrokinetic potential: Geophysics, **73**, no. 5, E165–180, doi: 10.1190/1.2959139.
- Schriever, W., and C. E. Bleil, 1957, Streaming potentials in spherical-grained sands: Journal of the Electrochemical Society, **104**, no. 3, 170–176, doi: 10.1149/1.2428528.
- Sen, P. N., and P. A. Goode, 1992, Influence of temperature on electrical conductivity on shaly sands: Geophysics, **57**, no. 1, 89–96, doi: 10.1190/1.1443191.
- Sen, P. N., C. Scala, and M. H. Cohen, 1981, Self-similar model for sedimentary rocks with application to the dielectric constant of fused glass beads: Geophysics, **46**, no. 5, 781–795, doi: 10.1190/1.1441215.
- Somasundaran, P., and R. D. Kulkarni, 1973, A new streaming potential ap-

- paratus and study of temperature effects using it: *Journal of Colloid and Interface Science*, **45**, no. 3, 591–600, doi: 10.1016/0021-9797(73)90176-8.
- Watanabe, T., and Y. Katagishi, 2006, Deviation of linear relation between streaming potential and pore fluid pressure difference in granular material at relatively high Reynolds numbers: *Earth, Planets, and Space*, **58**, 1045–1051.
- Watillon, A., and R. de Backer, 1970, Potentiel d'écoulement, courant d'écoulement et conductance de surface à l'interface eau-verre: *Journal of Electroanalytical Chemistry*, **25**, 181–196, doi: 10.1016/S0022-0728(70)80336-9.
- White, H. L., F. Urban, and E. T. Krick, 1932a, Stream potential determinations on glass capillaries of various sizes: *Journal of Physical Chemistry*, **36**, no. 1, 120–129, doi: 10.1021/j150331a008.
- White, H. L., F. Urban, and E. A. V. Atta, 1932b, A correlation of stream potentials and surface conductance: *Journal of Physical Chemistry*, **36**, no. 12, 3152–3156, doi: 10.1021/j150342a025.
- White, H. L., B. Monaghan, and F. Urban, 1936, Stream potentials, and d. c. surface conductivities in small capillaries: *Journal of Physical Chemistry*, **40**, no. 2, 207–214, doi: 10.1021/j150371a006.
- Wyllie, M. R. J., and A. R. Gregory, 1955, Fluid flow through unconsolidated porous aggregates: Effect of porosity and particle shape on the Kozeny-Carman constants of unconsolidated porous aggregates: *Industrial & Engineering Chemistry*, **47**, no. 7, 1379–1388, doi: 10.1021/ie50547a037.
- Yang, W.-C., 2003, *Handbook of fluidization and fluid-particle systems*: CRC Press.